International Geology Review

Occurrence of an Alaskan-type complex in the Middle Tianshan Massif, Central Asian Orogenic Belt: inferences from petrological and mineralogical studies

Ben-Xun Su [a] [b] , Ke-Zhang Qin [a] , Patrick Asamoah Sakyi [c] , Sanjeewa P.K. Malaviarachchi [d] , Ping-Ping Liu [a] [b] , Dong-Mei Tang [a] , Qing-Hua Xiao [a] , He Sun [a] , Yu-Guang Ma [e] & Qian Mao [e]

[a] Key Laboratory of Mineral Resources, Institute of Geology and Geophysics, Chinese Academy of Sciences, P.O. Box 9825, Beijing, 100029, China

[b] Graduate University of Chinese Academy of Sciences, Beijing, 100049, China

[c] Department of Earth Science, University of Ghana, P.O. Box LG 58, Legon-Accra, Ghana

[d] Research School of Earth Sciences, The Australian National University, Canberra, ACT, 0200, Australia

[e] State Key Laboratory of Lithospheric Evolution, Institute of Geology and Geophysics, Chinese Academy of Sciences, P.O. Box 9825, Beijing, 100029, China

Available online: 13 Jun 2011

PLEASE SCROLL DOWN FOR ARTICLE

Taylor & Francis
Taylor & Francis Group

Occurrence of an Alaskan-type complex in the Middle Tianshan Massif, Central Asian Orogenic Belt: inferences from petrological and mineralogical studies

Ben-Xun Su[a,b]*, Ke-Zhang Qin[a]*, Patrick Asamoah Sakyi[c], Sanjeewa P.K. Malaviarachchi[d], Ping-Ping Liu[a,b], Dong-Mei Tang[a], Qing-Hua Xiao[a], He Sun[a], Yu-Guang Ma[e] and Qian Mao[e]

[a]*Key Laboratory of Mineral Resources, Institute of Geology and Geophysics, Chinese Academy of Sciences, P.O. Box 9825, Beijing 100029, China;* [b]*Graduate University of Chinese Academy of Sciences, Beijing 100049, China;* [c]*Department of Earth Science, University of Ghana, P.O. Box LG 58, Legon-Accra, Ghana;* [d]*Research School of Earth Sciences, The Australian National University, Canberra, ACT 0200, Australia;* [e]*State Key Laboratory of Lithospheric Evolution, Institute of Geology and Geophysics, Chinese Academy of Sciences, P.O. Box 9825, Beijing 100029, China*

The Xiadong mafic–ultramafic complex lies in the central part of the Middle Tianshan Massif (MTM), along the southern margin of the Central Asian Orogenic Belt (CAOB). This complex is composed of dunite, hornblende (Hbl) clinopyroxenite, hornblendite, and Hbl gabbro. These rocks are characterized by adcumulated textures and variable alteration. Orthopyroxene is an extremely rare mineral in all rock units and plagioclase is absent in dunite and Hbl clinopyroxenite. Hbl, Fe-chromite, and Cr-magnetite are common phases. Olivines have forsterite (Fo) contents ranging from 92.3 to 96.6. Clinopyroxenes are Ca-rich, Ti-poor diopsides, and mostly altered to tremolites or actinolites. Chromites display low TiO_2 and Al_2O_3 contents and high Cr# and $Fe^{2+}/(Fe^{2+} + Mg)$ values. Primary and secondary Hbls show wide compositional variations. These petrological and mineralogical features as well as mineral chemistry are comparable to typical Alaskan-type complexes worldwide, which are widely considered to have formed above subduction zones. The chemistry of clinopyroxene and chromite supports an arc plate-tectonic origin for the Xiadong complex. Its confirmation as an Alaskan-type complex implies that the MTM, with Precambrian basement, was probably a continental arc during oceanic plate underflow and further supports the hypothesis of southward subduction of the Palaeozoic Junggar Ocean.

Keywords: Alaskan-type mafic–ultramafic complex; Central Asian Orogenic Belt; mafic–ultramafic complex; Middle Tianshan Massif; continental arc

Introduction

The Central Asian Orogenic Belt (CAOB), reflecting juvenile crustal growth, is the largest Phanerozoic orogen in the world, extending 7000 km E–W, from the Siberian Craton in the north to the Tarim Craton in the south (Figure 1A; Sengör *et al*. 1993, 2004; Hu *et al*. 2000; Jahn *et al*. 2000a, 2000b, 2004; Windley *et al*. 2007; Sun *et al*. 2008; Xiao *et al*. 2009). Its tectonic evolution has been attributed to subduction, accretion, and collision of an ocean-arc–microcontinent system in the Palaeo-Asian Ocean (Wu *et al*. 1996; Gao *et al*. 1998, 2006, 2009; Chen *et al*. 1999; Xia *et al*. 2004; Xiao *et al*. 2004, 2009; Lin *et al*. 2009).

The Chinese Tianshan Mountains occupy the southern part of the CAOB and are characterized by widely distributed mafic–ultramafic complexes, most of which have been identified as ophiolites or post-orogenic intrusions (Xiao *et al*. 1992; Qin *et al*. 2002; Zhou *et al*. 2004; Mao *et al*. 2008; Pirajno *et al*. 2008; Zhang *et al*. 2008; Sun 2009). A great number of Early Permian mafic–ultramafic complexes are exposed in the Eastern Tianshan and Beishan belts and in most host magmatic Ni–Cu sulphide deposits (Figure 1B; Qin *et al*. 2002, 2003, 2007; Han *et al*. 2004; Zhou *et al*. 2004; Chai *et al*. 2006, 2008; Han *et al*. 2006; Jiang *et al*. 2006; Mao *et al*. 2006; Sun *et al*. 2006, 2007; Mao *et al*. 2008; Pirajno *et al*. 2008; Su *et al*. 2009, 2010a, 2010b; Tang *et al*. 2009; Wang *et al*. 2009; Liu *et al*. 2010; Xiao *et al*. 2010).

Although multiple subduction events in the CAOB have produced abundant arc-related volcanic rocks and coeval intrusions, so far no study has reported evidence for Alaskan-type complexes, which are thought to have formed in subduction zone environments (e.g. Williams 1991; Saleeby 1992; Foley *et al*. 1997; Ayarza *et al*. 2000; Valli *et al*. 2004). We discovered a mafic–ultramafic complex in the Middle Tianshan Massif (MTM) and recognized it to be of Alaskan-type. To our knowledge, this is the first finding of such a complex in the southern margin of the CAOB.

Here we present a detailed description of the petrological and mineralogical features of the Xiadong mafic–ultramafic complex and compare it with typical

---
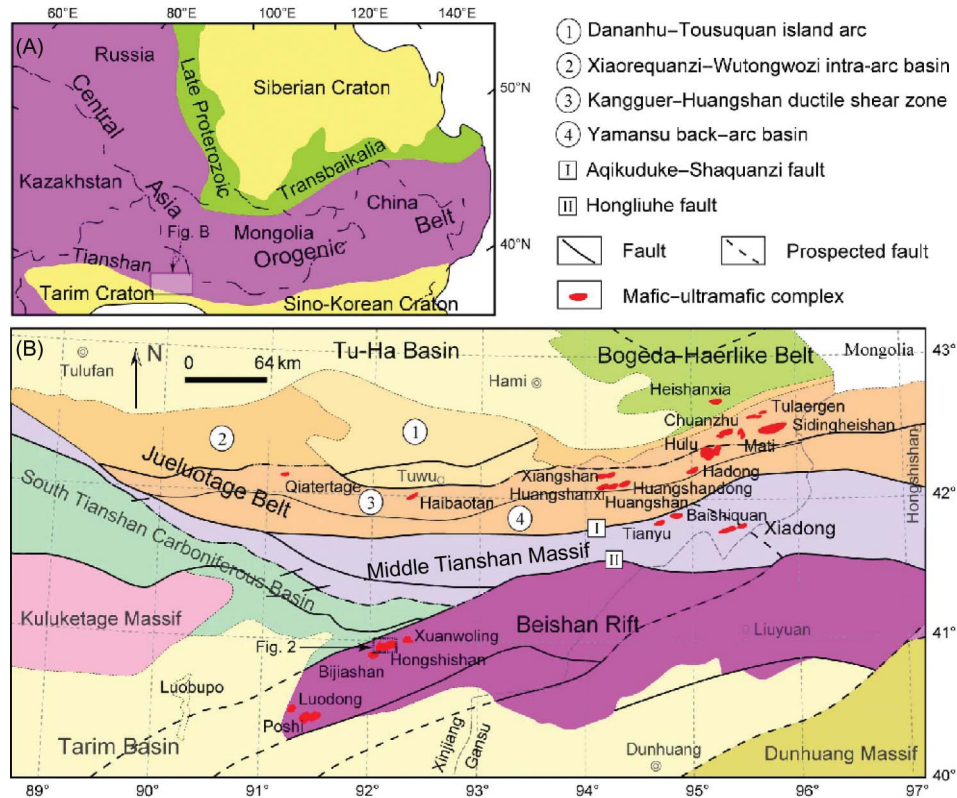
Figure 1. (A) Location map of the study area in the Central Asian Orogenic Belt and partly in the Tarim Craton (modified after Jahn *et al.* 2000b). (B) Regional geological map of the Eastern Tianshan and Beishan Rift showing the distribution of Palaeozoic mafic–ultramafic complexes (modified after Su *et al.* 2010a).

Alaskan-type complexes. These data are then used to shed light on the origin and emplacement of the complex.

Geological setting

The MTM, in eastern Xinjiang Uygur Autonomous Region, is situated between the Jueluotage tectonic belt in the north and the Beishan Rift in the south, and bounded by the Aqikuduke–Shaquanzi fault in the north and the Hongliuhe fault in the south (Figure 1B). Abundant granites and granitic gneisses crop out as a Precambrian crystalline basement of the MTM (BGMRXUAR 1993; Qin *et al.* 2002; Xu *et al.* 2009). Several Early Permian mafic–ultramafic complexes, including Tianyu (280 Ma; Su *et al.* 2010a) and Baishiquan (284.8 Ma; Su *et al.* 2010a), are distributed along the northern margin of the MTM. The Xiadong complex is located in the central part of the MTM (Figure 1B).

The Xiadong mafic–ultramafic complex is strip shaped and generally strikes E–W. It is 7 km long and up to 500 m wide with an exposed area of extent ~2.5 km^2 (Figure 2). The country rocks of the complex are dominated by late Proterozoic schist, gneiss, and marbles. Undated granite and diorite are widely present in the surrounding region and appear to be younger than the mafic–ultramafic complex,

as some granitic and dioritic veins intrude the mafic–ultramafic complex in the horizontal profile (Figure 2).

The rock types that compose the Xiadong complex are dunite, hornblende (Hbl) clinopyroxenite, Hbl gabbro, and minor hornblendite, hereafter called dunite, Hbl clinopyroxenite, Hbl gabbro, and hornblendite. The dunite body dominates the northern and western parts of the complex, whereas the Hbl clinopyroxenite and Hbl gabbro are mainly found in the southern and eastern parts. The hornblendite is only observed in the horizontal profile (Figure 2). The mafic rock units (Hbl clinopyroxenite, hornblendite, and Hbl gabbro) are mostly gradational over a short distance (approximately several metres), whereas the contacts within the dunite unit are well defined and display chilled margins (Figure 3A–3C). The profile demonstrates that many veins, including Hbl clinopyroxenite, Hbl gabbro, hornblendite, granite, and diorite, cut through the dunite bodies, suggesting late-stage intrusions within the dunite bodies.

Petrography

Dunite

The dunite occurs as bands of masses aligned in an E–W direction parallel to the elongated direction of the
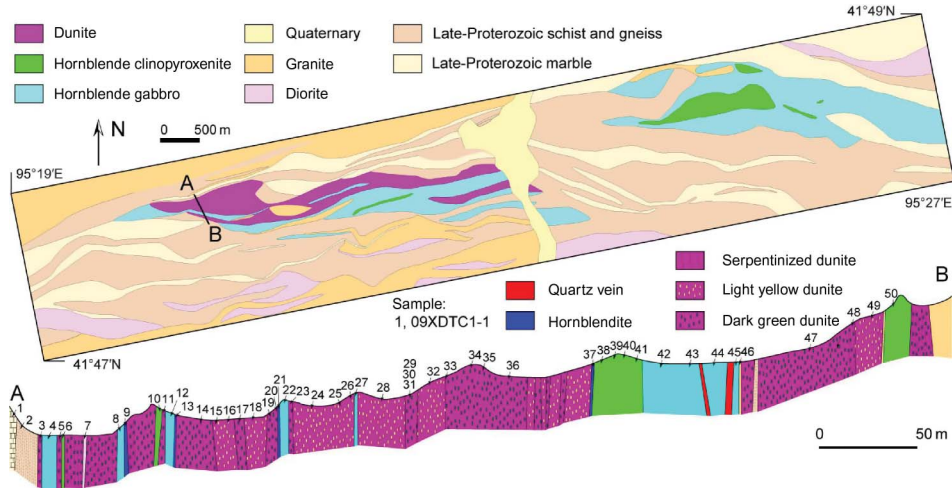
Figure 2. Geological map of the Xiadong mafic–ultramafic complex, accompanied by a horizontal profile along A to B showing its rock units and sampling positions.
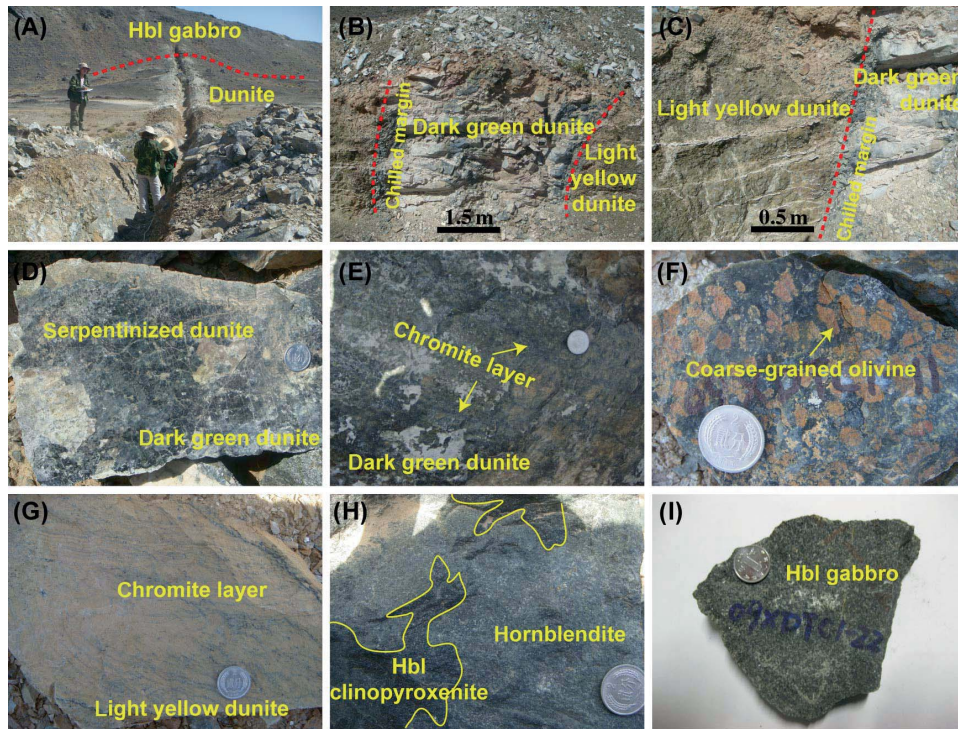
Figure 3. Field and outcrop photographs of the Xiadong mafic–ultramafic complex: (A) field survey showing the position of the horizontal profile and the relationship of dunite and Hbl gabbro; (B) light yellow dunite intruded by dark green dunite, with chilled margin present in the latter; (C) detailed contact between dark green dunite and light yellow dunite; (D) compact and the strongly serpentinized dark green dunite; (E) occurrence of chromite layer in dark green dunite; (F) coarse-grained, light yellow olivine aggregate within dark green dunite; (G) chromite layer well defined in light yellow dunite; (H) the contact between Hbl clinopyroxenite and hornblendite; (I) fresh Hbl gabbro sample.

Xiadong complex. It can be subdivided into two types: dark green dunite and light yellow dunite. The dark green dunite appears to be compact (Figure 3B and 3C) but essentially has been strongly serpentinized (Figure 3D). Most olivines in the dark green dunites are altered to

serpentines, whereas clinopyroxenes (modal abundance <5%) are replaced by actinolites or tremolites. Chromites with modal abundance of 5–10% display layered structure (Figure 3E) and preserve intact crystal shapes. Minor magnetites are observed as interstitial grains. At their contacts

with light yellow dunite bodies, the dark green dunite bodies frequently exhibit chilled margins ranging from 5 to 15 cm in width (Figure 3B and 3C). Some light yellow olivine aggregates can occasionally be observed in the dark green dunites (Figure 3F), probably demonstrating that the emplacement of the dark green dunite is later than that of the light yellow dunite.

The light yellow dunite consists of olivine and chromite with accessory Hbl and altered clinopyroxene. Olivines occur as cumulate crystals of variable sizes (Figure 4A). Many olivine grains are considerably large (2–4 mm) and irregularly shaped. Other olivine grains are small and round (<0.5 mm). Chromites occur as both interstitial and rhythmic layers (Figures 3G and 4A), where most chromite grains display elongated crystal shapes, whereas others have round shapes. Some chromites are present as inclusions or rims of spinels (Figure 5A). Most clinopyroxenes are long prismatic in shape with well-developed fractures (Figure 5A). Some clinopyroxene grains are altered to actinolite, tremolite, or chlorite (Figure 4A). Yellowish brown Hbls commonly form irregular patches rimming olivine and clinopyroxene.

Hbl clinopyroxenite

Hbl clinopyroxenite is mainly present within Hbl gabbro and can also be observed within dunite and hornblendite bodies in the horizontal profile (Figures 2 and 3H). It has a mineral assemblage of clinopyroxene, Hbl, and accessory magnetite and chromite. Cumulus clinopyroxenes are mostly altered to actinolite or tremolite, preserving a clinopyroxene core with Hbl rims (Figure 5B). Primary

Hbls are interstitial and commonly altered to actinolite along their rims. Magnetite and chromite grains are usually less than 40 μm, whereas dolomite is usually present as veins in the Hbl clinopyroxenites.

Hornblendite

Hornblendite occupies a minor lithology of the complex and is usually associated with Hbl clinopyroxenite and/or Hbl gabbro (Figures 2 and 3H). It consists of Hbl and plagioclase with accessory minerals such as magnetite, ilmenite, titanite, and chromite. Hbl crystals occur as cumulate and are mostly <0.5 mm in size. However, some Hbl grains are 2–4 mm in diameter and display recrystallized texture with fine-grained Hbls in their margins (Figure 5B). Plagioclase crystals in hornblendite are fine grained (<1 mm in size) and their modal abundance ranges from <5 to 15% (Figure 4B). The small amount of interstitial plagioclase is universally zoisitized. Accessory minerals occur as interstitial grains and are generally less than 0.4 mm in size. Titanite commonly occurs as rims around ilmenite.

Hbl gabbro

Hbl gabbro is the dominant rock type in the Xiadong mafic–ultramafic complex (Figure 2). It consists of a mineral assemblage of plagioclase, clinopyroxene, Hbl, magnetite, ilmenite, titanite, and apatite. Most Hbl gabbro samples show equigranular texture with mineral grains <1.5 mm in size (Figures 3I and 4C). Plagioclase is commonly zoisitized, whereas clinopyroxene and Hbl are
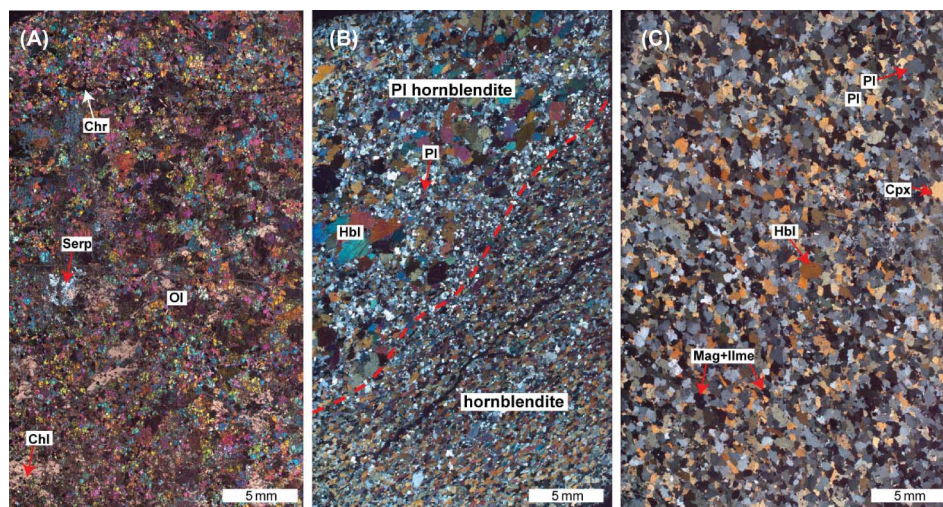
Figure 4. Microphotographs of the dunite, hornblendite, and Hbl gabbro samples from the Xiadong mafic–ultramafic complex: (A) the dunite sample (09XD-1) showing cumulate olivine and chromite with minor serpentine and chlorite; (B) the hornblendite sample (09XD-10) showing cumulate hornblende (Hbl) and recrystallized textured coarse Hbls, and heterogeneous distribution of plagioclase; (C) the Hbl gabbro sample (09XDTC1-22) exhibiting fine-grained texture with mineral assemblage of plagioclase, clinopyroxene, Hbl, magnetite, and ilmenite.
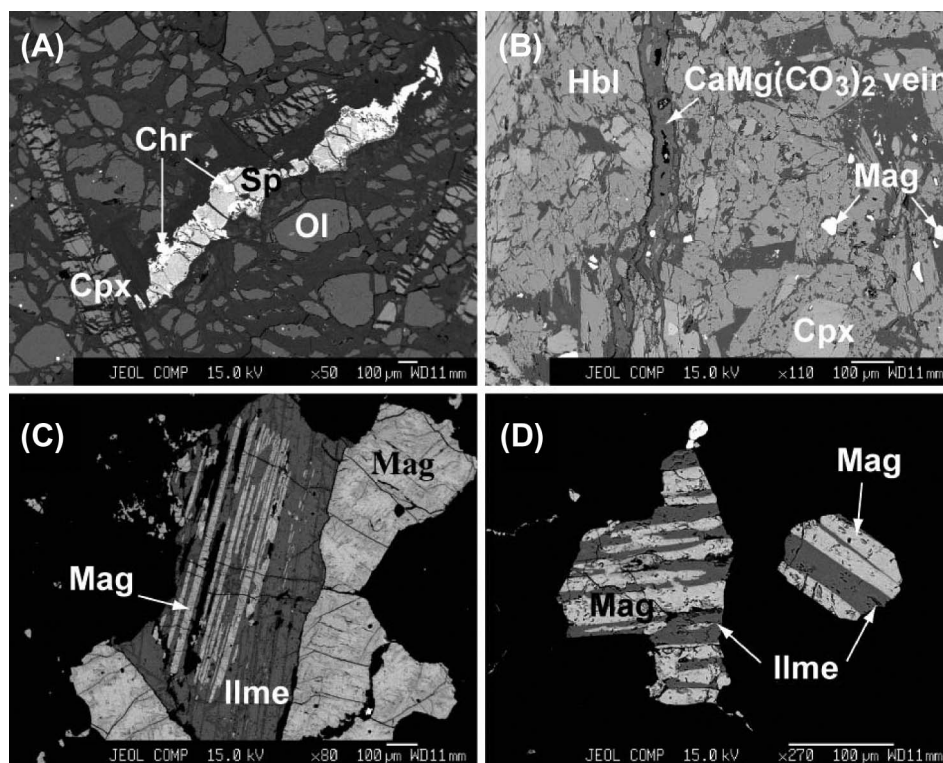
Figure 5. Back-scattered images of rocks from the Xiadong mafic–ultramafic complex. (A) Dunite 09XDTC1-28 showing fine-grained olivine, long prismatic clinopyroxene, spinel rimmed by chromite; (B) Hbl clinopyroxenite 09XDTC1-39 displaying altered clinopyroxene, primary hornblende (Hbl), granular magnetite, and dolomite vein; (C) Hbl gabbro 09XDTC1-12 showing the relationship between magnetite and ilmenite; (D) Hbl gabbro 09XDTC1-12 displaying detailed intergrowth of magnetite and ilmenite.

altered to actinolite or tremolite and contain ilmenite lamellae. The modal abundance of magnetite and ilmenite in the Hbl gabbros can reach up to 15%, which is relatively higher than that in other rock types (Figure 4C). The magnetites, in most cases, display parallel intergrowth with ilmenites and occasionally occur as interstitial grains (Figure 5C and 5D).

Analytical method

Quantitative mineral compositions were determined by wavelength-dispersive spectrometry using a JEOL JXA8100 electron probe (JEOL, Tokyo, Japan), operating at an accelerating voltage of 15 kV with 12 nA beam current, 5 μm beam spot, and 10–30 s counting time. The precisions of all analysed elements are better than 2.0%. Natural minerals and synthetic oxides were used as standards, and a program based on the ZAF procedure was used for data correction. The analyses were done at the State Key Laboratory of Lithospheric Evolution, Institute of Geology and Geophysics, Chinese Academy of Sciences. Fe^{2+}–Fe^{3+} redistribution from electron microprobe analyses was carried out using the general equation of Droop (1987) for estimating Fe^{3+}. Representative analyses of each of the analysed phases are given in Tables 1–6.

Mineral chemistry

Olivine

Olivine grains are only observed in the dunites of the Xiadong complex. They have Forsterite (Fo) ranging from 92.3 to 96.6, MnO from 0.03 to 0.23 wt.% with a range of 0.08–0.18 wt.%, NiO from 0.05 to 0.76 wt.%, and extremely low CaO of <0.04 wt.% (Table 1). The residual olivines in the strongly serpentinized dark green dunites show very similar compositions to those in the fresh light yellow dunites. The olivines in an individual sample are chemically homogeneous. MnO in olivine does not exhibit correlation with Fo number (Figure 6A). However, NiO and Fo show negative correlation (Figure 6B), which is different from their positive correlations in other olivines worldwide (Su *et al*. 2010c).

Chromite

Chromites normally occur as Fe-chromite and Cr-magnetite and two Al-spinel grains. The chromites have low Al_2O_3, TiO_2, and MgO contents in the range of 0.00–12.2 wt.%, 0.00–0.67 wt.%, and 0.24–6.68 wt.%, respectively. On the contrary, there are large Cr_2O_3 variations of 0.30–43.9 wt.% and high FeO contents of 65–96 wt.% (Table 2). The two spinel grains

Table 1. Olivine compositions of the Xiadong mafic–ultramafic complex.

Sample	Rock type	No.	SiO_2	TiO_2	Al_2O_3	Cr_2O_3	FeO	MnO	MgO	CaO	Na_2O	K_2O	NiO	Total	Fo
09XD-1	Dunite	6	41.8	0.03	0.00	0.00	4.85	0.16	53.3	0.00	0.00	0.01	0.27	100.5	95.2
09XDTC1-5	Dunite	4	41.2	0.00	0.00	0.05	5.67	0.11	51.8	0.03	0.01	0.00	0.51	99.4	94.3
09XDTC1-11	Dunite	5	41.7	0.00	0.00	0.00	7.28	0.09	50.9	0.02	0.00	0.01	0.47	100.4	92.6
09XDTC1-14	Dunite	5	41.9	0.03	0.00	0.01	6.36	0.10	51.3	0.01	0.00	0.00	0.76	100.4	93.6
09XDTC1-15	Dunite	5	39.9	0.02	0.00	0.06	5.60	0.07	53.0	0.00	0.00	0.02	0.35	99.0	94.5
09XDTC1-16	Dunite	5	41.0	0.00	0.00	0.02	4.98	0.14	53.3	0.00	0.00	0.00	0.34	99.7	95.1
09XDTC1-19	Dunite	5	41.5	0.00	0.01	0.00	6.92	0.16	51.2	0.00	0.00	0.00	0.50	100.3	93.0
09XDTC1-23	Dunite	5	42.0	0.00	0.01	0.00	6.45	0.14	51.6	0.01	0.00	0.01	0.41	100.7	93.5
09XDTC1-24	Dunite	5	42.1	0.00	0.00	0.03	3.64	0.08	53.6	0.01	0.04	0.02	0.29	99.8	96.4
09XDTC1-25	Dunite	4	42.4	0.05	0.00	0.00	3.59	0.14	54.1	0.02	0.02	0.00	0.32	100.7	96.4
09XDTC1-28	Dunite	5	42.4	0.01	0.00	0.00	4.36	0.12	53.5	0.03	0.00	0.02	0.48	100.9	95.7
09XDTC1-29	Dunite	5	42.2	0.00	0.00	0.04	4.04	0.14	53.2	0.03	0.02	0.02	0.44	100.1	96.0
09XDTC1-30	Dunite	5	42.4	0.00	0.00	0.01	3.62	0.11	54.3	0.00	0.00	0.00	0.28	100.7	96.4
09XDTC1-31	Dunite	5	42.1	0.02	0.00	0.02	5.75	0.17	52.2	0.01	0.00	0.00	0.11	100.4	94.2
09XDTC1-32	Dunite	5	42.0	0.00	0.01	0.00	3.55	0.11	53.9	0.02	0.01	0.01	0.23	99.9	96.5
09XDTC1-35	Dunite	4	42.1	0.00	0.00	0.09	5.00	0.19	53.1	0.04	0.01	0.03	0.36	100.8	95.0
09XDTC1-36	Dunite	5	42.3	0.06	0.00	0.00	4.15	0.19	53.9	0.00	0.01	0.03	0.32	100.9	95.9
09XDTC1-47	Dunite	5	41.8	0.03	0.00	0.01	6.99	0.12	51.6	0.01	0.00	0.01	0.42	100.9	93.0

Note: Fo = $100 \times Mg/(Mg + Fe)$.

have identical compositions in Al_2O_3 ($\sim$55.0 wt.%), Cr_2O_3 ($\sim$10.5 wt.%), FeO ($\sim$11.5 wt.%), and MgO ($\sim$12 wt.%). Most chromites have very low Mg# [$100 \times Mg/(Mg + Fe)$] values of <10 and very high Cr# [$100 \times Cr/(Cr + Al)$] values between 95 and 100. Several zoned chromites show relative enrichment of Al and Cr and depletion of Fe. The compositions of chromites are independent of their host rock types. In the ternary diagram of Fe^{3+}–Cr–Al, these chromites display an apparent Fe-enrichment trend (Figure 7A). Due to the extremely low Al_2O_3 contents, the chromites plot near the island-arc field and far away from the mid-ocean ridge basalt and Ocean island basalt fields in the Al_2O_3 versus TiO_2 diagram (Figure 7B).

Pyroxene

A very limited number of primary clinopyroxenes are present in the studied samples. Only one orthopyroxene grain is observed in the light yellow dunite sample (09XDTC1-14). The compositions of clinopyroxenes are all CaO-rich (24.6–25.7 wt.% except one grain of 20.1 wt.% in the sample 09XDTC1-40) and are subordinate to diopside (Table 3). Clinopyroxenes in the Hbl gabbros have variable amounts of SiO_2 (51.3–55.7 wt.%); low contents in TiO_2 (0.00–0.16 wt.%), Al_2O_3 (0.49–2.98 wt.%), FeO (0.51–1.29 wt.%), and Na_2O (0.03–0.33 wt.%); and extremely high Mg# (95.8–98.4). Clinopyroxenes in two Hbl clinopyroxenite samples show relatively low SiO_2 (50.6 wt.%, 50.5 wt.%) and Mg# (88.9, 84.5) and high TiO_2 (0.28 wt.%, 1.22 wt.%), Al_2O_3 (2.97 wt.%, 6.42 wt.%), and FeO (3.45 wt.%, 4.71 wt.%) (Table 3). These chemical characteristics of Ca enrichment and low Al, Ti, and Na are typical for clinopyroxenes from Alaskan-type complexes

(Snoke *et al*. 1981; Helmy and El Mahallawi 2003). Consequently, the Xiadong clinopyroxenes plot in the Alaskan-type Quetico complex fields in the diagrams of Al_2O_3 versus SiO_2 and TiO_2 versus Alz ($Al^{IV} \times 100/2$) (Figure 8A and 8B).

The orthopyroxene in the dunite is enstatite with Mg# of 94.2 and has high contents of SiO_2 (58.6 wt.%) and MgO (36.8 wt.%) and low Al_2O_3 (0.30 wt.%), FeO (4.05 wt.%), and CaO (0.05 wt.%) (Table 3).

Hornblende

Hbls in the dunites inherit precursory compositions of clinopyroxenes and occur as pargasite, magnesio-Hbl, and tremolite (Figure 9A), displaying wide compositional variations in SiO_2, Al_2O_3, FeO, and Na_2O (Table 4). The primary Hbls in the hornblendites are mainly pargasites and the secondary ones are magnesio-Hbls and tremolites (Figure 9A). The Hbls have slightly high contents of TiO_2, Al_2O_3, FeO, and Na_2O and low contents of SiO_2 and MgO (Table 4). Hbls in the Hbl clinopyroxenites are generally rich in MgO and poor in alkaline components (Na + K < 0.3; Figure 9B) and are classified as magnesio-Hbl and tremolite. The primary Hbls in the Hbl gabbros are mainly magnesio-Hbls with relatively homogeneous compositions, whereas the secondary ones formed after clinopyroxenes are rich in MgO and poor in Na_2O. The Hbls in one gabbroic diorite (09XDTC1-7) are mainly actinolites with homogeneous compositions (Table 4; Figure 9A). All the Hbls in the Xiadong complex exhibit negative correlations between Si and Na + K, consistent with the variations observed in typical Alaskan-type complexes (Figure 9B).

Table 2. Chromite compositions of the Xiadong mafic–ultramafic complex.

Sample	Rock type	Mineral	No.	SiO$_2$	TiO$_2$	Al$_2$O$_3$	Cr$_2$O$_3$	FeO	MnO	MgO	CaO	Na$_2$O	K$_2$O	NiO	Total	Cr#	Mg#
09XD-1	Dunite	Chr	4	0.01	0.22	0.04	14.1	80.7	0.57	2.25	0.00	0.01	0.00	0.81	98.7	99.6	4.73
09XDTC1-3	Dunite	Chr core	2	0.11	0.08	7.74	43.9	42.9	0.76	2.78	0.01	0.04	0.01	0.14	98.5	79.2	10.4
		Chr rim	1	0.02	0.50	0.29	36.7	58.2	0.84	1.41	0.02	0.02	0.00	0.23	98.2	98.8	4.14
09XDTC1-5	Dunite	Chr	3	0.02	0.24	0.09	22.9	70.9	0.89	2.75	0.01	0.00	0.00	0.72	98.5	99.4	6.46
09XDTC1-6	Hbl Cpxt	Chr	1	0.02	0.00	0.14	6.70	89.3	0.42	0.98	0.02	0.00	0.01	1.11	98.7	97.1	1.92
09XDTC1-11	Dunite	Chr core	2	0.01	0.67	0.15	20.9	75.3	0.76	1.07	0.00	0.04	0.01	0.62	99.5	98.9	2.46
		Chr rim	2	0.05	0.26	0.00	9.48	86.9	0.30	0.61	0.01	0.01	0.00	0.67	98.3	100.0	1.23
09XDTC1-14	Dunite	Chr	4	0.03	0.15	0.64	15.4	80.8	0.35	1.11	0.02	0.01	0.02	0.73	99.3	94.1	2.39
09XDTC1-15	Dunite	Chr	4	0.03	0.14	0.33	12.6	84.3	0.41	2.09	0.00	0.00	0.00	0.56	100.4	96.3	4.23
09XDTC1-16	Dunite	Chr	5	0.01	0.09	0.00	9.97	87.1	0.25	1.00	0.00	0.00	0.01	0.68	99.1	100.0	2.01
09XDTC1-19	Dunite	Chr	3	0.01	0.46	1.74	22.5	69.6	1.18	2.47	0.04	0.03	0.01	0.45	98.5	89.7	5.96
09XDTC1-20	Dunite	Chr	3	0.02	0.11	0.30	24.9	71.9	0.79	0.72	0.01	0.02	0.00	0.35	99.1	98.3	1.76
09XDTC1-23	Dunite	Chr	3	0.04	0.29	0.89	16.3	79.1	0.54	0.82	0.03	0.00	0.02	0.71	98.7	92.5	1.82
09XDTC1-24	Dunite	Chr	3	0.01	0.00	0.38	10.8	83.9	0.39	2.48	0.01	0.00	0.00	1.01	99.0	95.0	5.00
09XDTC1-25	Dunite	Chr	3	0.02	0.05	0.08	4.92	90.5	0.22	2.27	0.05	0.04	0.01	0.96	99.1	97.6	4.27
09XDTC1-28	Dunite	Sp	2	0.03	0.00	54.9	10.6	11.4	0.14	19.8	0.00	0.07	0.01	0.49	97.4	11.4	75.6
		Chr	3	0.01	0.27	0.14	12.5	83.0	0.48	1.56	0.01	0.00	0.01	1.02	99.0	98.4	3.24
09XDTC1-29	Dunite	Chr	4	0.00	0.12	0.04	7.54	88.1	0.26	1.31	0.00	0.02	0.00	0.86	98.3	99.1	2.58
09XDTC1-30	Dunite	Chr	3	0.00	0.16	1.62	28.2	64.9	1.01	2.78	0.02	0.03	0.02	0.57	99.3	92.1	7.09
09XDTC1-32	Dunite	Chr	3	0.01	0.16	1.08	20.1	74.0	0.65	3.48	0.00	0.00	0.00	0.64	100.1	92.6	7.73
09XDTC1-35	Dunite	Chr	3	0.06	0.14	0.05	1.38	96.2	0.05	0.49	0.00	0.02	0.01	0.37	98.8	95.1	0.89
09XDTC1-36	Dunite	Chr	3	0.02	0.18	0.03	14.6	80.6	0.52	2.01	0.00	0.00	0.00	0.73	98.7	99.7	4.25
09XDTC1-37	Hblt	Chr	2	0.01	0.40	0.08	13.9	81.5	0.46	0.82	0.00	0.01	0.00	0.57	97.8	99.2	1.76
09XDTC1-40	Hbl Cpxt	Chr	1	0.00	0.07	0.26	10.8	85.4	0.31	0.2	0.01	0.03	0.00	0.10	97.2	96.5	0.50
09XDTC1-47	Dunite	Chr	6	0.02	0.19	7.67	37.0	48.4	0.96	4.81	0.00	0.04	0.02	0.23	99.3	76.4	15.0
XDE-4	Hbl Gbr	Chr	2	2.43	0.00	11.2	51.9	23.9	2.54	4.43	0.35	0.05	0.35	0.00	97.2	75.7	24.8

Notes: Chr, chromite; Cpxt, clinopyroxenite; Gbr, gabbro; Hbl, hornblende; Hblt, hornblendite; Sp, spinel. Cr# = 100×Cr/(Cr + Al).

Table 3. Pyroxene compositions of the Xiadong mafic–ultramafic complex.

Sample	Rock type	Mineral	SiO_2	TiO_2	Al_2O_3	Cr_2O_3	FeO	MnO	MgO	CaO	Na_2O	K_2O	NiO	Total	Mg#	Fs	Wo	En
09XD-12	Hbl Cpxt	Cpx	50.6	0.28	2.97	0.05	3.45	0.10	15.4	24.7	0.05	0.00	0.03	97.6	88.9	5.49	50.4	44.1
09XDTC1-27	Hbl Gbr	Cpx	55.7	0.05	0.49	0.00	0.68	0.23	17.8	25.2	0.16	0.00	0.05	100.3	97.9	1.04	49.8	49.1
		Cpx	55.2	0.13	1.23	0.01	0.68	0.16	17.8	25.4	0.06	0.00	0.04	100.7	97.9	1.04	50.0	48.9
		Cpx	55.8	0.05	0.67	0.08	0.51	0.15	18.0	25.5	0.06	0.02	0.06	100.9	98.4	0.78	50.0	49.3
		Cpx	54.8	0.16	1.13	0.00	0.70	0.10	17.6	25.7	0.07	0.00	0.09	100.4	97.9	1.06	50.4	48.5
09XDTC1-40	Hbl Cpxt	Cpx	50.5	1.22	6.42	0.47	4.71	0.16	14.3	20.1	1.22	0.01	0.00	99.1	84.5	8.38	46.0	45.7
XDE-2	Hbl Gbr	Cpx	52.9	0.00	1.16	0.29	1.19	0.08	17.4	25.0	0.07	0.02	0.00	98.1	96.3	1.84	49.7	48.4
		Cpx	51.7	0.00	2.39	0.71	1.29	0.04	16.6	25.0	0.12	0.00	0.00	97.8	95.8	2.04	50.8	47.1
		Cpx	52.4	0.06	0.89	0.42	1.08	0.07	17.5	25.0	0.20	0.00	0.00	97.6	96.7	1.67	49.6	48.7
		Cpx	52.3	0.00	0.55	0.51	1.10	0.08	17.2	25.1	0.33	0.00	0.01	97.2	96.6	1.71	50.2	48.1
XDE-3	Hbl Gbr	Cpx	51.9	0.00	1.61	0.48	0.99	0.05	17.5	25.4	0.06	0.01	0.00	98.0	96.9	1.52	50.2	48.3
		Cpx	52.4	0.03	0.90	0.07	0.89	0.03	17.6	25.3	0.06	0.01	0.01	97.3	97.3	1.37	50.0	48.6
		Cpx	53.9	0.07	0.77	0.08	0.92	0.02	18.0	25.6	0.03	0.02	0.03	99.4	97.3	1.38	49.6	49.0
		Cpx	52.9	0.00	0.80	0.06	0.93	0.02	17.8	25.5	0.03	0.01	0.07	98.2	97.2	1.41	49.8	48.8
XDE-4	Hbl Gbr	Cpx	51.3	0.00	2.98	0.95	1.14	0.06	16.6	25.3	0.11	0.00	0.02	98.5	96.3	1.80	51.1	47.1
		Cpx	52.4	0.00	2.75	0.84	1.10	0.06	16.8	24.6	0.17	0.01	0.13	98.9	96.5	1.74	50.3	48.0
		Cpx	53.0	0.03	0.76	0.00	0.93	0.03	17.8	25.3	0.05	0.00	0.04	97.8	97.2	1.42	49.7	48.9
		Cpx	53.2	0.00	0.68	0.00	0.97	0.02	17.4	25.2	0.10	0.00	0.07	97.7	97.0	1.50	50.0	48.5
XDE-5	Hbl Gbr	Cpx	53.5	0.03	1.38	0.06	1.03	0.07	17.3	25.2	0.03	0.01	0.00	98.6	96.8	1.60	50.2	48.2
		Cpx	53.1	0.01	1.21	0.11	1.00	0.11	17.3	25.4	0.06	0.04	0.05	98.4	96.9	1.55	50.3	48.1
		Cpx	52.1	0.05	2.27	0.21	1.11	0.05	16.8	25.2	0.04	0.00	0.00	97.9	96.5	1.74	50.8	47.4
09XDTC1-14	Dunite	Opx	58.6	0.01	0.30	0.10	4.05	0.07	36.8	0.05	0.02	0.00	0.22	100.2	94.2	5.76	0.1	94.1

Notes: Cpx, clinopyroxene; Cpxt, clinopyroxenite; Gbr, gabbro; Hbl, hornblende; Opx, orthopyroxene. Mg# = $100 \times Mg/(Mg + Fe)$; Fs = $100 \times Fe/(Mg + Fe + Ca)$; Wo = $100 \times Ca/(Mg + Fe + Ca)$; En = $100 \times Mg/(Mg + Fe + Ca)$.

Table 4. Hbl compositions of the Xiadong mafic–ultramafic complex.

Sample	09XD-1		09XD-7	09XD-10	09XD-12	09XD-13	09XDTC2-1	XDZK1601-20	09XDTC1-4			09XDTC1-6	09XDTC1-7		09XDTC1-8	09XDTC1-9
Rock type	Dunite		Hblt	Hblt	Hbl Gbr	Hblt	Hblt	Hbl Gbr	Hbl Gbr			Hbl Cpxt	Gbr Dio		Hbl Gbr	Hblt
Mineral	Amph	Tr	Amph	Amph	Act	Amph	Amph	Amph	Amph	Act	Tr	Act	Act	Amph	Amph	Amph
No.	2	1	2	2	2	5	2	2	1	2	1	5	4	2	5	4
SiO_2	47.4	57.4	42.1	44.5	52.3	48.3	47.2	42.4	48.9	52.4	58.9	51.4	54.6	47.6	47.5	41.6
TiO_2	0.11	0.00	0.82	0.53	0.09	0.01	0.23	1.30	0.07	0.11	0.04	0.00	0.19	0.30	0.59	0.85
Al_2O_3	9.62	0.60	14.5	11.6	3.59	9.64	11.0	10.7	8.49	5.85	0.03	7.68	2.59	8.97	8.51	13.1
Cr_2O_3	0.64	0.09	0.23	0.04	0.11	0.02	0.22	0.00	0.86	0.29	0.00	0.07	0.02	0.03	0.03	0.00
FeO	3.56	0.76	10.9	16.1	6.31	3.69	4.84	18.0	3.94	3.38	0.96	3.50	9.95	12.2	13.4	15.8
MnO	0.09	0.09	0.26	0.25	0.14	0.07	0.09	0.44	0.08	0.07	0.14	0.05	0.24	0.16	0.28	0.25
MgO	19.4	24.7	13.3	11.5	19.0	18.7	17.7	10.3	20.0	21.0	23.9	19.8	17.2	14.1	13.4	10.3
CaO	12.2	12.3	12.2	10.5	12.5	12.3	13.0	11.5	12.0	12.0	13.2	13.1	11.9	11.8	11.6	11.7
Na_2O	2.37	0.04	2.38	2.00	0.36	1.51	1.48	1.32	2.04	1.34	0.01	1.31	0.60	1.73	1.14	1.84
K_2O	0.08	0.00	0.93	0.24	0.04	0.13	0.15	1.23	0.10	0.05	0.01	0.06	0.08	0.24	0.25	1.19
NiO	0.11	0.10	0.00	0.01	0.07	0.07	0.02	0.02	0.13	0.15	0.00	0.04	0.01	0.00	0.00	0.00
Total	95.6	96.0	97.6	97.3	94.5	94.4	96.0	97.1	96.6	96.7	97.3	97.0	97.4	97.2	96.6	96.6
Oxygen	23	23	23	23	23	23	23	23	23	23	23	23	23	23	23	23
Si	6.748	7.796	6.142	6.471	7.522	6.918	6.745	6.361	6.848	7.259	8.016	7.182	7.719	6.888	6.906	6.258
Ti	0.011	0.000	0.090	0.058	0.010	0.001	0.024	0.147	0.008	0.011	0.004	0.000	0.020	0.032	0.064	0.096
Al	1.613	0.096	2.490	1.989	0.609	1.628	1.854	1.884	1.402	0.955	0.005	1.266	0.431	1.530	1.458	2.321
Cr	0.072	0.010	0.027	0.004	0.013	0.003	0.025	0.000	0.096	0.031	0.000	0.008	0.002	0.003	0.003	0.000
Fe^{3+}	0.385	0.686	0.355	1.073	0.352	0.292	0.170	0.800	0.592	0.496	0.099	0.056	0.286	0.430	0.628	0.432
Fe^{2+}	0.039	0.599	0.976	0.883	0.406	0.150	0.408	1.451	0.130	0.104	0.010	0.353	0.891	1.044	1.000	1.552
Mn	0.011	0.011	0.032	0.031	0.017	0.008	0.010	0.056	0.009	0.008	0.016	0.006	0.028	0.019	0.034	0.031
Mg	4.120	5.002	2.888	2.490	4.071	4.000	3.763	2.301	4.176	4.343	4.850	4.129	3.622	3.052	2.907	2.310
Ca	1.859	1.792	1.909	1.633	1.920	1.891	1.986	1.839	1.799	1.786	1.926	1.967	1.810	1.833	1.802	1.888
Na	0.653	0.011	0.674	0.562	0.101	0.418	0.408	0.383	0.553	0.360	0.003	0.354	0.165	0.486	0.322	0.535
K	0.015	0.000	0.173	0.044	0.007	0.024	0.027	0.236	0.018	0.010	0.002	0.011	0.015	0.044	0.046	0.228
Ni	0.013	0.011	0.000	0.001	0.008	0.007	0.002	0.002	0.015	0.017	0.000	0.004	0.001	0.000	0.000	0.000
Total	15.54	14.81	15.76	15.24	15.04	15.34	15.42	15.46	15.38	15.17	14.93	15.34	14.99	15.36	15.17	15.65
Mg#	99.1	89.3	74.7	73.8	90.9	96.4	90.2	61.3	97.0	97.7	99.8	92.1	80.3	74.5	74.4	59.8

(continued)

Table 4.   (continued).

Sample	09XDTC1-10		09XDTC1-12	09XDTC1-13	09XDTC1-19	09XDTC1-21	09XDTC1-22		09XDTC1-24	09XDTC1-25	09XDTC1-28	09XDTC1-31	09XDTC1-32
Rock type	Hbl Cpxt		Hbl Gbr	Hblt	Dunite	Hblt	Hbl Gbr		Dunite	Dunite	Dunite	Dunite	Dunite
Mineral	Act	Tr	Amph	Amph	Amph	Amph	Amph	Act	Tr	Tr	Amph	Act	Act
No.	4	2	4	4	3	5	4	4	6	4	3	5	1
SiO$_2$	53.5	58.6	46.0	45.0	45.5	41.3	47.0	55.3	57.7	56.6	48.2	54.7	54.2
TiO$_2$	0.19	0.00	1.20	0.82	0.32	1.19	0.98	0.14	0.00	0.04	0.17	0.02	0.12
Al$_2$O$_3$	4.68	0.34	9.04	11.3	11.5	14.1	8.51	1.42	2.18	2.78	10.1	4.16	4.47
Cr$_2$O$_3$	0.00	0.00	0.04	0.03	0.42	0.04	0.05	0.00	0.11	0.06	0.61	0.00	0.09
FeO	3.43	1.63	14.8	11.9	4.80	13.3	13.2	9.20	1.64	1.91	4.01	2.55	2.48
MnO	0.11	0.17	0.44	0.33	0.08	0.32	0.31	0.29	0.09	0.06	0.03	0.08	0.05
MgO	21.5	23.5	12.0	13.9	18.9	12.0	13.4	17.7	23.1	22.9	19.5	22.2	22.0
CaO	12.0	12.7	11.3	11.1	11.7	11.9	11.4	12.5	12.8	12.6	12.5	12.4	12.4
Na$_2$O	1.21	0.10	1.83	2.26	2.67	2.42	1.51	0.21	0.35	0.38	1.74	0.87	0.76
K$_2$O	0.05	0.00	0.35	0.20	0.14	0.66	0.24	0.03	0.05	0.00	0.14	0.03	0.07
NiO	0.02	0.03	0.00	0.04	0.12	0.06	0.00	0.00	0.07	0.08	0.16	0.05	0.02
Total	96.8	97.0	96.9	96.8	96.1	97.3	96.7	96.8	98.0	97.4	97.2	97.1	96.7
Oxygen	23	23	23	23	23	23	23	23	23	23	23	23	23
Si	7.383	7.981	6.783	6.509	6.436	6.095	6.856	7.865	7.799	7.685	6.727	7.489	7.446
Ti	0.020	0.000	0.133	0.089	0.034	0.132	0.108	0.015	0.000	0.004	0.018	0.002	0.013
Al	0.761	0.055	1.570	1.922	1.914	2.446	1.463	0.238	0.348	0.446	1.666	0.671	0.725
Cr	0.000	0.000	0.004	0.003	0.047	0.004	0.005	0.000	0.012	0.006	0.067	0.000	0.010
Fe^{3+}	0.540	0.258	0.448	0.773	0.766	0.514	0.558	0.130	0.215	0.377	0.508	0.476	0.471
Fe^{2+}	0.145	0.072	1.375	0.672	0.197	1.127	1.056	0.965	0.030	0.159	0.040	0.184	0.186
Mn	0.013	0.020	0.055	0.040	0.010	0.040	0.038	0.035	0.011	0.007	0.003	0.009	0.006
Mg	4.427	4.759	2.631	2.993	3.991	2.641	2.916	3.753	4.646	4.634	4.051	4.536	4.516
Ca	1.778	1.846	1.778	1.715	1.774	1.876	1.788	1.905	1.858	1.837	1.868	1.811	1.830
Na	0.324	0.027	0.523	0.634	0.733	0.691	0.426	0.058	0.091	0.101	0.471	0.232	0.203
K	0.008	0.000	0.065	0.036	0.024	0.125	0.044	0.005	0.008	0.000	0.025	0.006	0.011
Ni	0.003	0.003	0.000	0.004	0.014	0.007	0.000	0.000	0.007	0.009	0.018	0.005	0.002
Total	15.11	14.88	15.37	15.39	15.55	15.70	15.26	14.97	14.96	14.95	15.38	15.05	15.05
Mg#	96.8	98.5	65.7	81.7	95.3	70.1	73.4	79.5	99.4	96.7	99.0	96.1	96.1

Table 4. (continued).

Sample	09XDTC1-37	09XDTC1-39		09XDTC1-40	09XDTC1-42	XDE-1	XDE-2		XDE-3	XDE-4	XDE-5	XDE-5
Rock type	Hblt	Hbl Cpxt		Hbl Cpxt	Hblt	Hbl Gbr	Hbl Gbr		Hbl Gbr	Hbl Gbr	Hbl Gbr	Hbl Gbr
Mineral	Act	Amph	Tr	Tr	Amph	Amph	Amph	Act	Amph	Amph	Amph	Act
No.	5	6	2	2	1	3	1	3	5	5	3	1
SiO_2	53.3	48.4	56.8	57.5	46.5	47.9	44.4	53.9	46.7	50.7	47.7	52.5
TiO_2	0.05	0.23	0.06	0.03	0.45	0.03	0.00	0.03	0.01	0.07	0.02	0.04
Al_2O_3	2.46	8.36	0.03	0.11	9.33	8.09	13.9	2.42	11.5	7.18	10.5	3.91
Cr_2O_3	0.01	0.13	0.02	0.00	0.00	0.37	1.95	0.70	0.56	1.04	1.08	0.03
FeO	9.21	3.91	0.82	1.22	12.8	3.78	2.87	1.46	2.09	1.89	2.19	1.67
MnO	0.18	0.04	0.08	0.08	0.24	0.09	0.07	0.05	0.05	0.08	0.07	0.08
MgO	17.6	19.8	24.1	23.4	13.7	19.5	17.3	22.3	19.1	20.6	19.5	22.1
CaO	12.4	13.3	13.2	13.1	12.3	12.6	13.1	13.5	13.0	13.2	12.8	13.1
Na_2O	0.62	0.62	0.05	0.07	1.01	1.24	2.08	0.19	1.69	1.09	1.56	0.46
K_2O	0.03	0.06	0.00	0.00	0.30	0.10	0.21	0.03	0.32	0.12	0.23	0.13
NiO	0.00	0.05	0.07	0.00	0.00	0.05	0.14	0.07	0.00	0.08	0.06	0.06
Total	95.9	94.9	95.2	95.5	96.8	93.7	96.0	94.6	95.1	96.0	95.8	94.0
Oxygen	23	23	23	23	23	23	23	23	23	23	23	23
Si	7.667	6.881	7.899	7.987	6.776	6.915	6.378	7.632	6.680	7.135	6.741	7.456
Ti	0.006	0.024	0.006	0.004	0.049	0.003	0.000	0.003	0.002	0.007	0.002	0.004
Al	0.416	1.403	0.005	0.018	1.602	1.376	2.351	0.404	1.929	1.191	1.751	0.654
Cr	0.001	0.015	0.003	0.000	0.000	0.042	0.221	0.078	0.063	0.116	0.121	0.004
Fe^{3+}	0.234	0.531	0.220	0.090	0.559	0.484	0.000	0.083	0.125	0.101	0.270	0.270
Fe^{2+}	0.873	0.066	0.124	0.051	1.006	0.027	0.344	0.090	0.125	0.122	0.011	0.072
Mn	0.022	0.005	0.010	0.010	0.030	0.011	0.008	0.006	0.007	0.009	0.008	0.009
Mg	3.780	4.208	4.982	4.841	2.980	4.196	3.698	4.704	4.070	4.319	4.118	4.675
Ca	1.911	2.024	1.967	1.946	1.925	1.943	2.011	2.046	1.996	1.985	1.945	1.996
Na	0.174	0.172	0.013	0.018	0.284	0.347	0.579	0.051	0.467	0.298	0.426	0.125
K	0.005	0.011	0.001	0.001	0.056	0.018	0.039	0.005	0.059	0.022	0.041	0.023
Ni	0.000	0.005	0.007	0.000	0.000	0.006	0.016	0.008	0.000	0.009	0.007	0.006
Total	15.09	15.21	14.99	14.96	15.27	15.31	15.65	15.11	15.52	15.31	15.42	15.15
Mg#	81.2	98.5	97.6	99.0	74.8	99.4	91.5	98.1	97.0	97.3	99.7	98.5

Note: Act, actinolite; Amph, amphibole; Cpxt, clinopyroxenite; Dio, diorite; Gbr, gabbro; Hbl, hornblende; Hblt, hornblendite; Tr, tremolite.

Table 5. Plagioclase compositions of the Xiadong mafic–ultramafic complex.

Sample	Rock type	Mineral	No.	SiO$_2$	TiO$_2$	Al$_2$O$_3$	Cr$_2$O$_3$	FeO	MnO	MgO	CaO	Na$_2$O	K$_2$O	NiO	Total	An	Ab
09XD-7	Hblt	Pl	2	64.2	0.06	21.2	0.00	0.01	0.02	0.03	2.07	10.7	0.21	0.00	98.5	9.72	90.3
		Zo	2	43.0	0.02	23.6	0.01	0.10	0.00	0.00	26.2	0.12	0.00	0.03	93.1	99.2	0.81
09XD-10	Hblt	Pl	2	58.5	0.00	24.8	0.04	0.03	0.00	0.00	6.57	7.97	0.02	0.00	98.0	31.3	68.7
09XD-13	Hbl Gbr	Zo	4	43.5	0.03	33.7	0.00	0.01	0.01	0.00	17.7	1.07	0.02	0.00	96.2	90.1	9.86
XDZK1601-20	Hbl Gbr	Pl	1	59.3	0.00	24.5	0.00	0.02	0.00	0.00	6.42	7.94	0.07	0.01	98.2	30.9	69.1
09XDTC1-7	Gbr Dio	Pl	3	66.6	0.04	20.5	0.12	0.04	0.03	0.03	1.69	10.9	0.05	0.00	100.1	7.86	92.1
09XDTC1-8	Hbl Gbr	Pl	2	60.5	0.07	24.4	0.00	0.08	0.03	0.01	6.30	8.24	0.03	0.02	99.7	29.7	70.3
09XDTC1-12	Hbl Gbr	Pl	3	62.4	0.00	23.4	0.00	0.04	0.00	0.01	4.86	8.99	0.06	0.00	99.8	23.0	77.0
09XDTC1-21	Hblt	Zo	4	38.6	0.13	25.7	0.05	8.92	0.15	0.05	23.2	0.00	0.00	0.00	96.7	99.9	0.02
09XDTC1-22	Hbl Gbr	Pl	3	62.8	0.00	23.6	0.00	0.06	0.00	0.01	5.00	8.99	0.09	0.04	100.6	23.5	76.5
09XDTC1-27	Hbl Gbr	Zo	5	39.0	0.12	27.0	0.00	7.11	0.09	0.03	23.5	0.01	0.01	0.00	96.9	99.9	0.08
XDE-1	Hbl Gbr	Zo	2	44.4	0.00	32.8	0.02	0.02	0.04	0.00	16.6	1.87	0.02	0.00	95.7	83.1	16.9
XDE-2	Hbl Gbr	Zo	6	38.7	0.02	32.5	0.17	0.37	0.00	0.04	24.0	0.01	0.00	0.00	95.8	99.9	0.07
XDE-3	Hbl Gbr	Zo	3	38.4	0.00	33.0	0.03	0.66	0.01	0.03	24.4	0.01	0.01	0.01	96.5	99.9	0.04
XDE-4	Hbl Gbr	Zo	2	39.0	0.00	32.1	0.02	0.75	0.04	0.03	24.0	0.00	0.01	0.02	95.9	100	0.00
XDE-5	Hbl Gbr	Zo	2	38.4	0.02	33.1	0.01	0.46	0.03	0.03	23.9	0.01	0.00	0.01	96.0	99.9	0.10

Notes: Dio, diorite; Hbl, hornblende; Hblt, hornblendite; Gbr, gabbro; Pl, plagioclase; Zo, zoisite. An = $100 \times$ Ca/(Ca + Na); Ab = $100 \times$ Na/(Ca + Na).

Table 6. Ilmenite and titanite compositions of the Xiadong mafic–ultramafic complex.

Sample	Rock type	Mineral	SiO$_2$	TiO$_2$	Al$_2$O$_3$	Cr$_2$O$_3$	FeO	MnO	MgO	CaO	Na$_2$O	K$_2$O	NiO	Total
09XDTC1-7	Gbr Dio	Tita	30.8	38.2	0.85	0.03	0.76	0.01	0.04	27.8	0.00	0.02	0.00	98.5
09XDTC1-8	Hbl Gbr	Ilme	0.00	52.0	0.00	0.02	42.9	3.86	0.10	0.06	0.00	0.01	0.00	98.9
		Tita	31.0	39.2	0.57	0.04	0.39	0.04	0.02	28.1	0.01	0.00	0.00	99.4
09XDTC1-12	Hbl Gbr	Ilme	0.03	51.3	0.00	0.02	43.1	4.36	0.10	0.05	0.03	0.00	0.00	99.0
		Ilme	0.02	49.0	0.02	0.05	45.9	2.67	0.41	0.04	0.02	0.00	0.02	98.1
09XDTC1-13	Hblt	Ilme	0.02	50.8	0.00	0.04	41.9	6.20	0.10	0.05	0.00	0.03	0.00	99.1
		Tita	30.8	39.2	0.64	0.01	0.35	0.06	0.00	28.3	0.00	0.00	0.04	99.3
09XDTC1-21	Hblt	Ilme	0.03	49.7	0.01	0.02	41.3	7.47	0.15	0.03	0.02	0.01	0.03	98.8
		Tita	30.8	37.3	1.59	0.00	0.83	0.06	0.00	28.4	0.02	0.00	0.00	99.0
09XDTC1-22	Hbl Gbr	Ilme	0.03	49.4	0.01	0.00	45.9	2.88	0.10	0.04	0.03	0.01	0.00	98.4
		Ilme	0.00	49.7	0.00	0.05	47.3	1.68	0.08	0.01	0.00	0.00	0.03	98.8

Note: Dio, diorite; Gbr, gabbro; Hbl, hornblende; Hblt, hornblendite; Ilme, ilmenite; Tita, titanite.
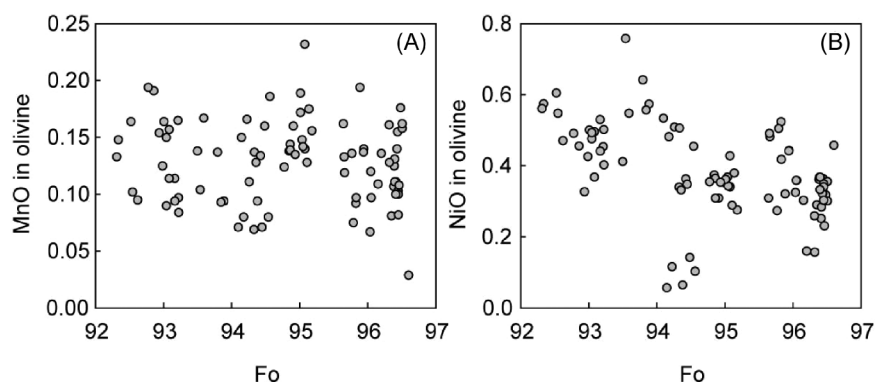
Figure 6. Plots of (A) Fo versus MnO and (B) Fo versus NiO contents of olivines in the Xiadong mafic–ultramafic complex.
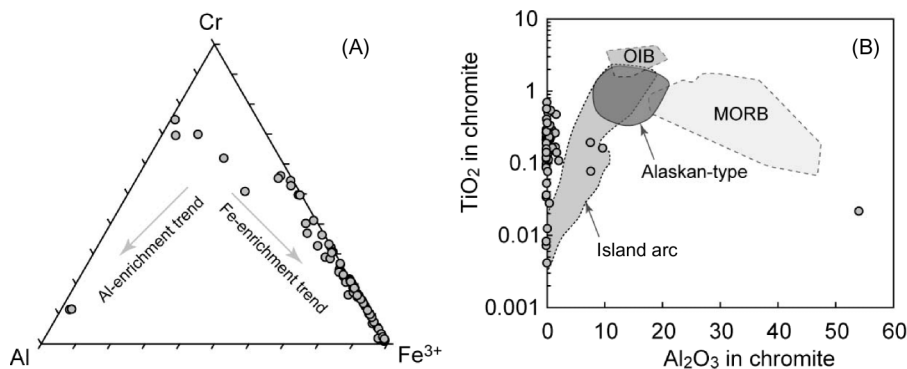
Figure 7. Plots of chromite compositions in the Xiadong mafic–ultramafic complex. (A) Fe^{3+}–Cr–Al diagram demonstrating Fe-enrichment trend; (B) Al$_2$O$_3$ versus TiO$_2$ diagram showing the close relationship between the Xiadong chromites and the island-arc field. Alaskan-type field after Alaska complex (Himmelberg *et al*. 1986; Himmelberg and Loney 1995); Ocean island basalt (OIB), mid-ocean ridge basalt (MORB), and island-arc fields after Kamenetsky *et al*. (2001).

Plagioclase

Plagioclases are completely absent in the dunites and Hbl clinopyroxenites, and those present in some hornblendites and Hbl gabbros are strongly affected by alteration, changing to mostly zoisites. These zoisites have apparent Ca enrichment and Si–Al–Na depletion. Some relics of

primary plagioclases have anorthite (An) numbers between 9.72 and 30.9 (Table 5).

Ilmenite and titanite

Ilmenites are commonly present in hornblendites and Hbl gabbros and have TiO$_2$ in the range of 49.0–52.0 wt.%,
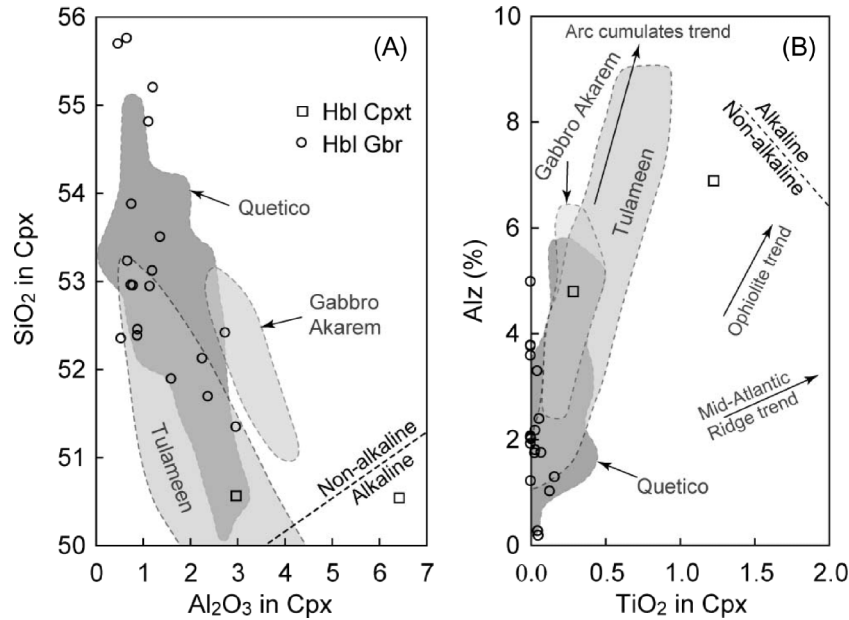
Figure 8.   Plots of clinopyroxene compositions in the Xiadong mafic–ultramafic complex. (A) Al_2O_3 versus SiO_2 and (B) TiO_2 versus Alz in clinopyroxene. The fields of the Alaskan-type complexes are from Quetico, Pettigrew and Hattori (2006); Tulameen, Rublee (1994); and Gabbro Akarem, Helmy and El Mahallawi (2003). Non-alkaline and alkaline boundary is after Le Bas (1962) and Alz refers to the percentage of Al in the tetrahedral sites $(100 \times Al^{IV})/2$. The arc cumulate, ophiolite, and Mid-Atlantic Ridge trends are after Loucks (1990).
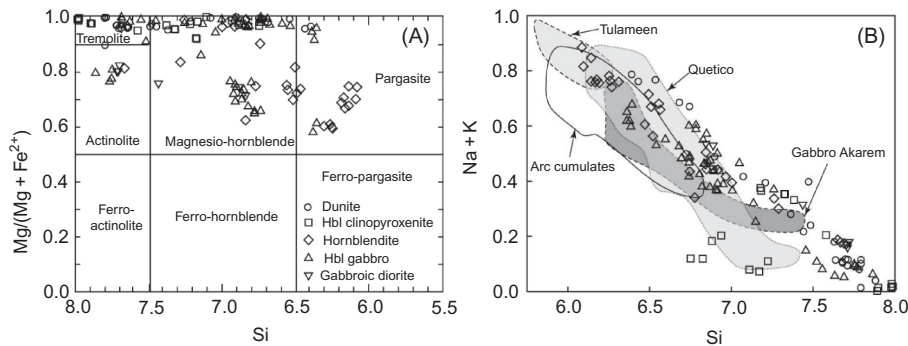
Figure 9.   Plots of hornblende (Hbl) compositions in the Xiadong mafic–ultramafic complex. (A) Hbl classification after Leake *et al*. (1997); (B) Si versus Na + K contents in Hbl. The fields of the Alaskan-type complexes are from Quetico, Pettigrew and Hattori (2006); Tulameen, Rublee (1994); and Gabbro Akarem, Helmy and El Mahallawi (2003). Arc cumulates field is defined by Beard and Barker (1989).

FeO of 41.3–47.3 wt.%, and MnO of 1.68–7.47 wt.%. All the analysed titanites show homogeneous compositions (Table 6).

Discussion

Comparisons to regional mafic–ultramafic complexes

Abundant mafic–ultramafic complexes are distributed in the Jueluotage Belt, MTM, and Beishan Rift (Figure 1B). These complexes from the three belts have apparently

different features. The Jueluotage and MTM complexes are generally composed of clinopyroxene/Hbl peridotite, olivine clinopyroxenite, clinopyroxenite, gabbro, norite, and diorite. These rocks often exhibit poikilitic and gabbroic textures. Orthopyroxene, plagioclase, and mica are common minerals, but magnetite is minor or absent in these complexes. Fo contents of olivines range from 78 to 86. Clinopyroxenes are classified as diopside and augite. Spinels are mainly Al-rich types and no chromite is observed. Most of the complexes host magmatic Ni–Cu sulphide deposits (Qin *et al*. 2003, 2007; Zhou *et al*. 2004;

Chai *et al*. 2006, 2008; Mao *et al*. 2008; Pirajno *et al*. 2008; Liu *et al*. 2010; Xiao *et al*. 2010).

The rock types of the Beishan complexes are mainly dunite, clinopyroxene peridotite, troctolite, gabbro, and diorite. Plagioclase is present in all rock units, but orthopyroxene and hydrous minerals such as Hbl and mica are completely absent. Very rare magnetite is observed. Poikilitic (orthocumulated) and gabbroic textures are also well developed in the ultramafic and mafic rocks, respectively. Olivines have Fo contents in the range of 76–90. Clinopyroxenes are diopsidic and augitic and spinels range from Al-spinel to Cr-spinel. Significant amounts of disseminated Ni–Cu sulphides have also been observed in these complexes (Jiang *et al*. 2006; Su *et al*. 2009, 2010a, 2010b; Ao *et al*. 2010).

These regional mafic–ultramafic complexes have widely been interpreted as evolving from high-Mg tholeiitic magmas from the lithospheric mantle in the postorogenic extension tectonic setting and/or mantle plume (Zhou *et al*. 2004; Han *et al*. 2006; Jiang *et al*. 2006; Wang *et al*. 2006; Chai *et al*. 2008; Mao *et al*. 2008; Pirajno *et al*. 2008; Zhang *et al*. 2008; Su *et al*. 2009, 2010a, 2010b; Sun 2009). The Xiadong complex, on the contrary, is distinctly different in petrology, mineralogy, and mineral chemistry from other regional complexes, suggesting that the petrogenesis and tectonic environment for the evolution of the Xiadong complex is different from the other two.

Comparisons to classic Alaskan-type complexes

Typical features of Alaskan-type complexes have been well documented in previous studies (e.g. Taylor 1967; Irvine 1974; Rublee 1994; Himmelberg and Loney 1995; Johan 2002; Helmy and El Mahallawi 2003; Pettigrew and Hattori 2006; Thakurta *et al*. 2008; Ripley 2009). Morphologically, Alaskan-type complexes have crude concentric zoning in lithologies and, in most cases, are roughly circular or elliptical in shape, pipe-like in cross section, with sizes ranging from 12 to 14 km^2 (Johan 2002). Petrologically, the Alaskan-type complexes are generally composed of dunite, wehrlite, olivine clinopyroxenite, Hbl clinopyroxenite, hornblendite, and Hbl gabbro, but the complete sequence of lithologies is rarely observed (Irvine 1974; Himmelberg and Loney 1995). The ultramafic cumulates tend to show adcumulated textures and lack interstitial minerals crystallized from 'trapped liquid' (Thakurta *et al*. 2008; Ripley 2009). Mineralogically, abundant clinopyroxenes and primary Hbls occur in Hbl clinopyroxenites and hornblendites. Chromite is commonly concentrated in dunite and often forms stratiform segregations and irregular veins (Irvine 1974; Himmelberg and Loney 1995; Johan 2002; Ripley 2009). Orthopyroxene and plagioclase are rare in the ultramafic rocks, and plagioclase occurs only in marginal gabbroic rocks (Helmy and El Mahallawi 2003; Pettigrew and Hattori 2006). Magnetite is a common mineral in clinopyroxenite and hornblendite and its modal abundance can range between ∼15 and 20% (Taylor 1967; Himmelberg and Loney 1995).

The mineral chemistry of Alaskan-type complexes is characterized by Mg-rich olivine, Ca-rich diopsidic clinopyroxene, high Fe–Cr, and low Al chromite, and calcic Hbls with a wide range in composition (Irvine 1974; Rublee 1994; Helmy and El Mahallawi 2003). Geochemically, all rock types show low abundances of incompatible elements such as Y and rare earth elements, low high-field strength elements, and relatively high large-ion lithophile elements (Helmy and El Mahallawi 2003; Pettigrew and Hattori 2006; Ripley 2009).

The Xiadong mafic–ultramafic complex has rock units of dunite, Hbl clinopyroxenite, hornblendite, and Hbl gabbro, together with a mineral assemblage of high-Mg olivine, diopsidic clinopyroxene, chromite, calcic Hbl, magnetite, and other accessory minerals, which are identical to typical Alaskan-type complexes. On the contrary, the regional mafic–ultramafic complexes in the Eastern Tianshan and Beishan Rift can be excluded from the Alaskan-type complexes.

Chromite compositions are important indicators to distinguish an Alaskan-type complex, stratiform complex, Alpine-type complex, and ophiolite. Relative to Alaskan-type complexes, chromites from both stratiform and Alpine-type complexes have higher Mg#, lower $Fe^{3+}/(Fe^{3+} + Cr + Al)$ ratios, and slightly lower Cr# (Figure 10A and 10B; Irvine 1967); whereas the chromites from ophiolites show apparently lower $Fe^{2+}/(Mg + Fe^{2+})$ ratios (Figure 10C; Barnes and Roeder 2001). All chromites from the Xiadong complex overlap with the field defined by the typical Alaskan-type complexes and display similar compositional trends to Alaskan-type complexes (Figure 10A–10C). Furthermore, it is apparent that chromite compositions of the Xiadong complex follow a differentiation (Fe enrichment) trend from an intermediate Cr–Al-rich spinel to Cr-magnetite (Figure 7A). Such trend of increasing Fe^{3+} has been reported for spinels from Alaskan-type complexes (Snoke *et al*. 1981; Nixon *et al*. 1990) and is not identified with other igneous complexes such as ophiolites or layered intrusions (Barnes and Roeder 2001). Clinopyroxenes and Hbls from the Xiadong complex also have compositional variations similar to some Alaskan-type complexes such as Quetico, Tulameen, and Gabbro Akarem (Figures 8A, 8B, and 9B). Olivines from Alaskan-type complexes worldwide show a Fo range from 66 to 95 (Figure 11). The Xiadong olivines show anomalously high Fo contents in the range of 92–97, partly overlapping the range of those from typical Alaskan-type complexes (Figure 11). All the comparisons are summarized in Table 7.
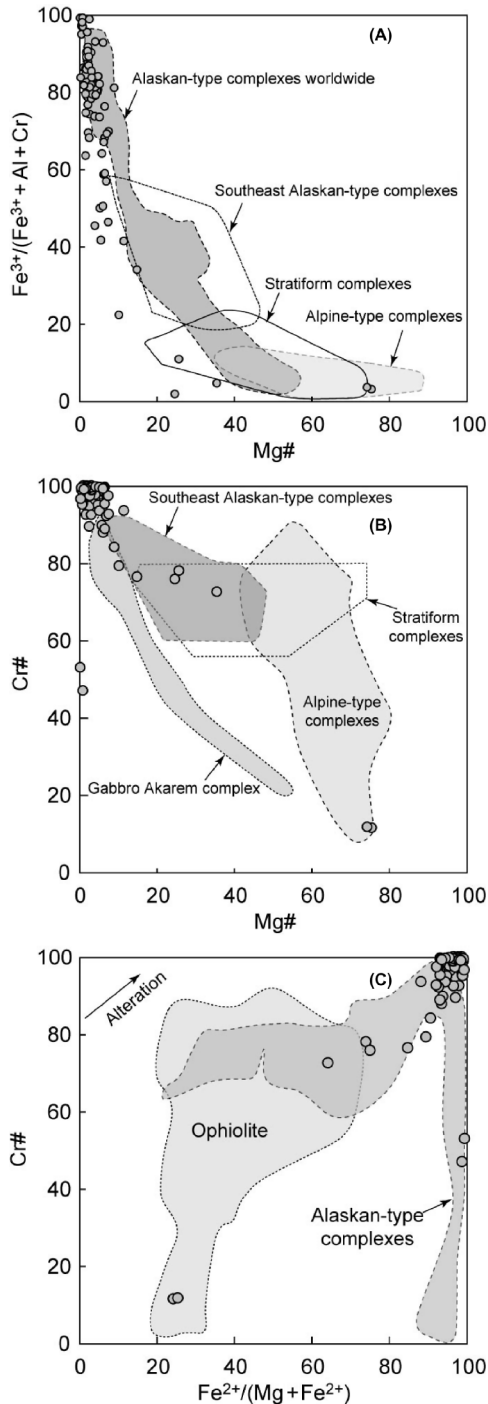
Figure 10. Chromite compositional comparisons between Xiadong and typical Alaskan-type complexes. (A) Plot of Mg# versus $Fe^{3+}/(Fe^{3+} + Al + Cr)$ of chromites. The fields in the diagram are from Alaskan-type complexes worldwide, Barnes and Roeder (2001); SE Alaskan-type complexes, stratiform complexes, and Alpine-type complexes, Irvine (1967). (B) Plot of Mg# versus Cr# of chromites. All field sources are the same as in (A). (C) Plot of $Fe^{2+}/(Mg + Fe^{2+})$ versus Cr# of chromites. The fields of Alaskan-type complexes and ophiolite and alteration trend are after Barnes and Roeder (2001).
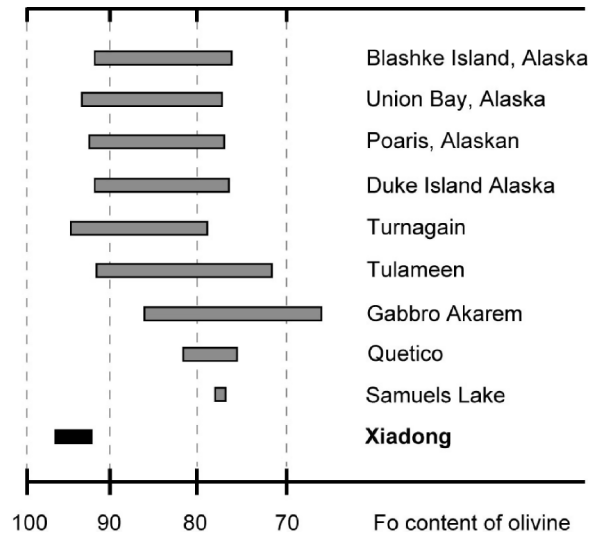
Figure 11. Fo content of olivines from the Xiadong mafic–ultramafic complex and typical Alaskan-type complexes (modified after Pettigrew and Hattori 2006). Sources: Turnagain, Clark (1980); Gabbro Akarem, Helmy and Moggesie (2001); Blashke Island, Himmelberg *et al*. (1986); Union Bay, Polaris, and Duke Island, Irvine (1974, 1976), Tulameen, Rublee (1994); Quetico and Samuel Lake, Pettigrew and Hattori (2006).

These similarities suggest that the Xiadong complex is equivalent to an Alaskan-type complex in terms of petrology and mineral chemistry, indicating that they are probably cogenetic, but without any similarity to stratiform, Alpine-type, and ophiolitic complexes.

Petrogenesis and tectonic significance

A number of hypotheses have been proposed to account for the Alaskan-type complexes. Taylor (1967) suggested that fractional melting in the mantle accounted for Alaskan-type complexes. Sha (1995) proposed that the parental magmas of Alaskan-type complexes fractionally crystallized from the mixture between a mantle-derived mafic magma and a crustal felsic magma. Efimov (1998), on the contrary, attributed Alaskan-type complexes to tectonic emplacement of fragments of a pre-existing body. Farahat and Helmy (2006) suggested the formation of Alaskan-type complexes by fractional crystallization from a common hydrous parental magma without significant crustal contamination. Parental magmas of the Xiadong complex most likely contain high Mg contents, evidenced by anomalously high-Fo olivine (Table 1; Figure 6), high-Mg# clinopyroxene (Table 3), and high-Mg Hbl (Table 4; Figure 9A). On the contrary, olivines only occur in the dunite unit, and their compositions do not show fractional correlations but homogeneous MnO contents against varying Fo and negative correlation between NiO and Fo (Table 6). The discontinuity of mineral modal abundances and intrusive contacts with chilled margins (Figures 2, 3B, and 3C) suggests that

Table 7. Comparisons between typical Alaskan-type and Xiadong complexes.

	Alaskan-type complexes	Xiadong complexes
Age	Mostly Phanerozoic	Late Carboniferous*
Geological setting	Close to the end of subduction, prior to accretion–collision	Close to the end of subduction, prior to accretion–collision*
Size	Most are small in size ranging from 12 to 40 km^2	In size of ∼2.5 km^2
Morphology and zoning	Crude concentric zoning of lithologies grading from olivine-rich ultramafic cores to mafic rims	Strip shape
Sequence of intrusion	Gabbroic and dioritic rocks intrude late	Gabbroic and dioritic rocks intrude late
Lithology	Dunite, hornblendite, clinopyroxenite, gabbro; minor dioritic and syenitic rocks	Dunite, hornblendite, Hbl clinopyroxenite, Hbl gabbro; minor diorite and no syenite
Textures	Accumulated texture with minor/no trapped liquid	Accumulated texture with minor/no trapped liquid
Mineralogy	Abundant clinopyroxene, primary hornblende, magnetite; lack of orthopyroxene and plagioclase in ultramafic rocks	Abundant clinopyroxene, primary hornblende, magnetite; lack of orthopyroxene and plagioclase in ultramafic rocks
Chromite	Common occurrence of chromite in dunite	Common occurrence of chromite in dunite
Mineral chemistry	High-Mg olivine; diopsidic clinopyroxene; phlogopitic mica; hornblende is calcic with a wide range in composition	High-Mg olivine, diopsidic clinopyroxene; hornblende is calcic with a wide range in composition
Bulk rock geochemistry	Low incompatible elements; relatively high LILE and low HFSE; no Eu anomalies	Relatively high LILE, and low HFSE and REE; no Eu anomalies*
Mineralization	PGE mineralization in olivine-rich cores (dunite) associated with chromite; rare Cu–Ni mineralization	Showing potential PGE mineralization in dunite; no Cu–Ni sulphide mineralization*

Notes: Hbl, hornblende; HFSE, high field strength element; LILE, large-ion lithophile element; PGE, platinum group element; REE, rare earth element. The features of Alaskan-type complexes are after Taylor (1967), Irvine (1974), Rublee (1994), Johan (2002), Helmy and El Mahallawi (2003), Pettigrew and Hattori (2006), Thakurta *et al*. (2008), and Ripley (2009). Those marked '*' will be shown elsewhere.

the Xiadong complex was formed by multi-stage emplacement of magma, in the sequence of light yellow dunite, dark green dunite, Hbl clinopyroxenite, hornblendite, and finally Hbl gabbro. In the genesis stage of dunites, Mn, Ni, and Fe are probably preferentially partitioned into chromites as evidenced by the negative correlation of MnO and the positive correlation of NiO in chromites with the Fo contents of olivines (Figure 12). Fe^{3+}-enrichment trend in chromites (Figure 7A) and associated ilmenite (Figure 5C and 5D) possibly imply that they were crystallized in a relatively high oxidizing environment. A considerable number of dolomite veins observed in the Xiadong rocks (Figure 5B) indicates that the complex most likely has reacted with its country rocks such as marble during its emplacement.

Alaskan-type complexes are always related to the subduction environment and arc accretion (Taylor 1967; Irvine 1974). For example, the complexes in Alaska intruded the western margin of the North American continent during the closure of the intra-arc basin (Saleeby 1992; Foley *et al*. 1997; Thakurta *et al*. 2008; Ripley 2009); the Ural mafic–ultramafic complexes intruded during the accretion of arc terrane to the continent (Ayarza *et al*. 2000); the Quetico complex formed through the accretion of micro-continents and arcs to the north, through the subduction of intervening oceanic crust (Williams 1991; Valli *et al*. 2004; Farahat and Helmy 2006). In this study, however, the MTM and Jueluotage Belt subduction events took place in Palaeozoic (Han *et al*. 2006; Wang *et al*. 2006; Zhang *et al*. 2008)

and the Dananhu–Tousuquan, Xiaorequanzi–Wutongwozi, and Yamansu are recognized to be island-arc basin, intra-arc basin, and back-arc basin, respectively (Figure 1B; Qin *et al*. 2002). Thus, the identification of the Xiadong complex as an Alaskan-type intrusion implies that the MTM with Precambrian basement was probably a continental arc during the subduction process. This tectonic framework may indicate that the Palaeozoic Junggar Ocean located to the north of the MTM (Ma *et al*. 1993; Qin *et al*. 2002; Li 2004; Zhang *et al*. 2004, 2008; Han *et al*. 2006; Li *et al*. 2006a, 2006b; Wang *et al*. 2006).

Conclusion

We have conducted a comprehensive study of the petrology, mineralogy, and mineral chemistry of the Xiadong mafic–ultramafic complex. The complex has identical mineral chemistry, as well as similar petrological and mineralogical characteristics as typical Alaskan-type complexes worldwide. The relationships between the rock units, modal compositions of minerals, and chemical compositional variations indicate that the Xiadong complex was formed by multi-stage emplacement mechanisms, accompanied by reaction with the surrounding country rocks. The discovery and the confirmation of the Xiadong complex as an Alaskan-type complex imply that the MTM with Precambrian basement was most likely a continental arc
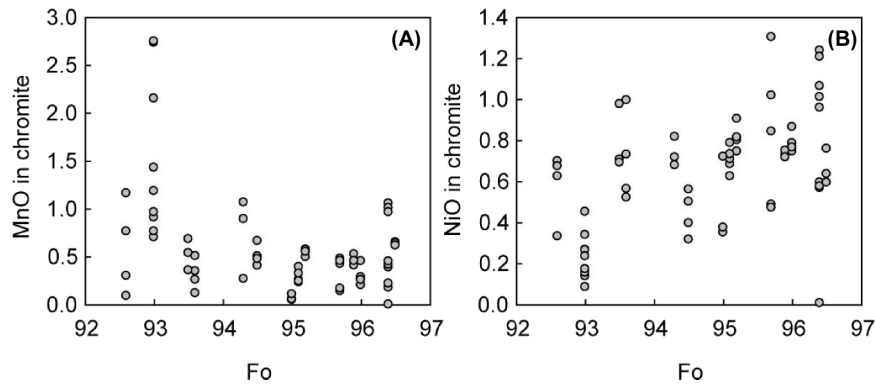
Figure 12.   Plots of (A) Fo versus MnO and (B) Fo versus NiO of chromites and olivines from the Xiadong mafic–ultramafic complex.

during the subduction of oceanic lithosphere, which further supports the hypothesis of southward underflow of the Palaeozoic Junggar Ocean.

References

Ao, S.J., Xiao, W.J., Han, C.M., Mao, Q.G., and Zhang, J.E., 2010, Geochronology and geochemistry of Early Permian mafic-ultramafic complexes in the Beishan area, Xinjiang, NW China: Implications for late Paleozoic tectonic evolution of the southern Altaids: Gondwana Research, doi: 10.1016/j.gr.2010.01.004.

Ayarza, P., Brown, D., Alvarez-Marron, J., and Juhlin, C., 2000, Contrasting tectonic history of the arc-continent suture in the southern and middle Urals: Implications for the evolution of the orogen: Journal of Geological Society, London, v. 157, p. 1065–1076.

Barnes, S.J., and Roeder, P.L., 2001, The range of spinel compositions in terrestrial mafic and ultramafic rocks: Journal of Petrology, v. 12, p. 2279–2302.

Beard, J.S., and Barker, F., 1989, Petrology and tectonic significance of gabbros, tonalities, shoshonites, and anorthosites in a late Paleozoic arc-root complex in the Wrangellia terrane, southern Alaska: Journal of Geology, v. 97, p. 667–683.

BGMRXUAR (Bureau of Geology and Mineral Resources of Xinjiang Uygur Autonomous Region), 1993, Regional Geology of Xinjiang Uygur Autonomous Region: Beijing, Geological Publishing House, p. 1–841 (in Chinese).

Chai, F.M., Zhang, Z.C., Mao, J.W., Dong, L.H., Zhang, Z.H., and Wu, H., 2008, Geology, petrology and geochemistry of the Baishiquan Ni-Cu-bearing mafic-ultramafic intrusions in Xinjiang, NW China: Implications for tectonics and genesis of ores: Journal of Asian Earth Sciences, v. 32, p. 218–235.

Chai, F.M., Zhang, Z.C., Mao, J.W., Dong, L.H., Zhang, Z.H., Ye, H.T., Wu, H., and Mo, X.H., 2006, Petrography and mineralogy of Baishiquan Cu-Ni-bearing mafic-ultramafic intrusions in Xinjiang: Acta Petrologica et Mineralogica, v. 25, p. 1–12 (in Chinese with English abstract).

Chen, C.M., Lu, H.F., Jia, D., Cai, D.S., and Wu, S.M., 1999, Closing history of the southern Tianshan oceanic basin, Western China: An oblique collisional orogeny: Tectonophysics, v. 302, p. 23–40.

Clark, T., 1980, Petrology of the Turnagain ultramafic complex, northwestern British Colombia: Canadian Journal of Earth Science, v. 17, p. 744–757.

Droop, G.T.R., 1987, A general equation for estimating Fe^{3+} concentrations in ferromagnesian silicates and oxides from microprobe analyses, using stoichiometric criteria: Mineralogical Magazine, v. 51, p. 431–435.

Efimov, A.A., 1998, The platinum belt of the Urals: Structure, petrogenesis, and correlation with platiniferous complexes of the Aldan Shield and Alaska, *in* Proceedings of the 8th International Platinum Symposium (Abstract), South Africa, p. 93–96.

Farahat, E.S., and Helmy H.M., 2006, Abu Hamamid Neoproterozoic Alaskan-type complex, south Eastern Desert, Egypt: Journal of African Earth Sciences, v. 45, p. 187–197.

Foley, J.P., Light, T.D., Nelson, S.W., and Harris, R.A., 1997, Mineral occurrences associated with mafic-ultramafic and related alkaline complexes in Alaska: Economic Geology, v. 9, p. 396–449.

Gao, J., Li, M.S., Xiao, X.C., Tang, Y.Q, and He, G.Q., 1998, Paleozoic tectonic evolution of the Tianshan orogen, northwestern China: Tectonophysics, v. 287, p. 213–231.

Gao, J., Long, L.L., Klemd, R., Qian, Q., Liu, D.Y., Xiong, X.M., Su, W., Liu, W., Wang, Y.T., and Yang F.Q., 2009, Tectonic evolution of the South Tianshan orogen and adjacent regions, NW China: Geochemical and age constraints of granitoid rocks: International Journal of Earth Sciences, v. 98, p. 1221–1238.

Gao, J., Long, L.L., Qian, Q., Huang, D.Z., Su, W., and Klemd, R., 2006, South Tianshan: A late Paleozoic or a Triassic orogen: Acta Petrologica Sinica, v. 22, p. 1049–1061 (in Chinese with English abstract).

Han, B.F., Ji, J.Q., Song, B., Chen, L.H., and Li, Z.H., 2004, SHRIMP zircon U-Pb ages of Kalatongke No. 1 and Huangshandong Cu-Ni-bearing mafic-ultramafic complexes, North Xinjiang, and geological implications: Chinese Science Bulletin, v. 49, p. 2424–2429.

Han, C.M., Xiao, W.J., Zhao, G.C., Mao, J.W., Li, S.Z., Yan, Z., and Mao, Q.G., 2006, Major types, characteristics and geodynamic mechanism of upper Paleozoic copper deposits in northern Xinjiang, northwestern China: Ore Geology Reviews, v. 28, p. 308–328.

Helmy, H.M., and El Mahallawi, M.M., 2003, Gabbro Akarem mafic–ultramafic complex, Eastern Desert, Egypt: A late Precambrian analogue of Alaskan-type Complexes: Mineralogy and Petrology, v. 77, p. 85–108.

Helmy, H.M., and Moggesie, A., 2001, Gabbro Akarem, Eastern Desert, Egypt: Cu-Ni-PGE mineralization in a concentrically zoned mafic-ultramafic complex: Mineralium Deposita, v. 36, p. 58–71.

Himmelberg, G.R., and Loney, R.A., 1995, Characteristics and petrogenesis of Alaskan-type ultramafic-mafic intrusions, Southeastern Alaska: US Geological Survey, Professional Papers 1564, Washington, D.C., U.S. Government Printing Office, p. 1–47.

Himmelberg, G.R., Loney, R.A., and Craig, J.T., 1986, Petrogenesis of the ultramafic complex at the Blashke Islands, Southern Alaska: US Geological Survey Bulletin 1662, Washington, D.C., U.S. Government Printing Office, p. 1–14.

Hu, A.Q., Jahn, B.M., Zhang, G., Chen, Y., and Zhang, Q., 2000, Crustal evolution and Phanerozoic crustal growth in northern Xinjiang: Nd isotope evidence. 1. Isotopic characterization of basement rocks: Tectonophysics, v. 328, p. 15–51.

Irvine, T.N., 1967, The Duke Island ultramafic complex, south-eastern Alaska, in Wyllie, P.J., ed., Ultramafic and Related Rocks: New York, John Wiley and Sons, p. 84–97.

Irvine, T.N., 1974, Petrology of the Duke Island ultramafic complex southern Alaska: Geological Society of American Memoir, v. 138, p. 240.

Irvine, T.N., 1976, Alaskan-type ultramafic-gabbro bodies in the Aiken Lake, McConnel Creek, and Toodagoone map-areas: Geological Survey of Canadian Paper, v. 76-1A, p. 76–81.

Jahn, B.M., Windley, B., Natal'in, B., and Dobretsov, N., 2004, Phanerozoic continental growth in Central Asia: Journal of Asian Earth Sciences, v. 23, p. 599–603.

Jahn, B.M., Wu, F.Y., and Chen, B., 2000a, Massive granitoid generation in Central Asia: Nd isotope evidence and implication for continental growth in the Phanerozoic: Episodes, v. 23, p. 82–92.

Jahn, B.M., Wu, F.Y., and Chen, B., 2000b, Granitoids of the Central Asian Orogenic Belt and continental growth in the Phanerozoic: Research of Society Edinburgh: Earth Science, v. 91, p. 181–193.

Jiang, C.Y., Cheng, S.L., Ye, S.F., Xia, M.Z., Jiang, H.B., and Dai, Y.C., 2006, Lithogeochemistry and petrogenesis of Zhongposhanbei mafic rock body, at Beishan region, Xinjiang: Acta Petrologica Sinica, v. 22, p. 115–126 (in Chinese with English abstract).

Johan, Z., 2002, Alaskan-type complexes and their platinum-group element mineralization, in Cabri, L.J., ed., Geology, geochemistry, mineralogy and mineral beneficiation of platinum-group elements: Canadian Institute of Mining, Metallurgy and Petroleum, Quebec, special v. 54, p. 669–719.

Kamenetsky, V.S., Crawford, A.J., and Meffre, S., 2001, Factors controlling chemistry of magmatic spinel: An empirical study of associated olivine, Cr-spinel and melt inclusions from primitive rocks: Journal of Petrology, v. 42, p. 655–671.

Leake, B.E., Woolley, A.R., Arps, C.E.S., Birch, W.D., Gilbert, M.C., Grice, J.D., Hawthorne, F.C., Kato, A., Kisch, H.J., Krivovichev, V.G., Linthout, K., Laird, J., Mandarino, J.A., Maresch, W.V., Nickel, E.H., Rock, N.M.S., Schumacher, J.C., Smith, D.C., Stephenson, N.C.N., Ungaretti, L., Whittaker, E.J.W., and Guo, Y.Z., 1997, Nomenclature of amphiboles: Report of the subcommittee on amphiboles of the international mineralogical association, commission on new minerals and mineral names: The Canadian Mineralogist, v. 35, p. 219–246.

Le Bas, M.J., 1962, The role of aluminum in igneous clinopyroxenes with relation to their parentage: American Journal of Sciences, v. 260, p. 267–288.

Li, J.Y., 2004, Late Neoproterozoic and Paleozoic tectonic framework and evolution of eastern Xinjiang, NW China: Geological Review, v. 50, p. 304–322 (in Chinese with English abstract).

Li, J.Y., Song, B., Wang, K.Z., Li, Y.P., Sun, G.H., and Qi, D.Y., 2006a, Permian mafic-ultramafic complexes on the southern margin of the Tu-Ha Basin, east Tianshan Mountains: Geological records of vertical crustal growth in central Asia: Acta Geoscientica Sinica, v. 27, p. 424–446 (in Chinese with English abstract).

Li, J.Y., Wang, K.Z., Sun, G.H., Mo, S.G., Li, W.Q., Yang, T.N., and Gao, L.M., 2006b, Paleozoic active margin slices in the southern Turfan-Hami basin: Geological records of subduction of the Paleo-Asian Ocean plate in central Asian regions: Acta Petrologica Sinica, v. 22, p. 1087–1102 (in Chinese with English abstract).

Lin, W., Faure, M., Shi, Y.H., Wang, Q.C., and Li, Z., 2009, Palaeozoic tectonics of the south-western Chinese Tianshan: New insights from a structural study of the high-pressure/low-temperature metamorphic belt: International Journal of Earth Sciences, v. 98, p. 1259–1274.

Liu, P.P., Qin, K.Z., Su, S.G., San, J.Z., Tang, D.M., Su, B.X., Sun, H., and Xiao, Q.H., 2010, Characteristics of multi-phase sulfide droplets and their implications for conduit-style mineralization of Tulargen Cu-Ni deposit, Eastern Tianshan, Xinjiang: Acta Petrologica Sinica, v. 26, p. 523–532 (in Chinese with English abstract).

Loucks, R.R., 1990, Discrimination of ophiolitic from nonophiolitic ultramafic-mafic allochthons in orogenic belts by the Al/Ti ration in clinopyroxene: Geology, v. 18, p. 346–349.

Ma, R.S., Wang, C.Y., Ye, S.F., and Liu, G.B., 1993, Tectonic framework and crustal evolution of the Eastern Tianshan: Nanjing, Nanjing University Press (in Chinese).

Mao, J.W., Pirajno, F., Zhang, Z.H., Chai, F.M., Wu, H., Chen, S.P., Cheng, S.L., Yang, J.M., and Zhang, C.Q., 2008, A review of the Cu-Ni sulfide deposits in the Chinese Tianshan and Altay orogens (Xinjiang Autonomous Region, NW China): Principal characteristics and ore-forming processes: Journal of Asian Earth Sciences, v. 32, p. 184–203.

Mao, Q.G., Xiao, W.J., Han, C.M., Sun, M., Yuan, C., Yan, Z., Li, J.L., Yong, Y., and Zhang, J.E., 2006, Zircon U-Pb age and geochemistry of the Baishiquan mafic-ultramafic complex in the Eastern Tianshan, Xinjiang: Constraints on the closure of the Paleo-Asian Ocean: Acta Petrologica Sinica, v. 22, p. 153–162 (in Chinese with English abstract).

Nixon, G.T., Cabri, L.J., and Laflamme, J.H.G., 1990, Platinum group element mineralization in lode and placer deposits associated with the Tulameen Alaskan-type complex, British Columbia: Canadian Mineralogist, v. 28, p. 503–535.

Pettigrew, N.T., and Hattori, K.H., 2006, The Quetico intrusions of Western Superior Province: Neo-Archean examples of Alaskan/Ural-type mafic-ultramafic intrusions: Precambrian Research, v. 149, p. 21–42.

Pirajno, F., Mao, J.W., Zhang, Z.C., Zhang, Z.H., and Chai, F.M., 2008, The association of mafic-ultramafic intrusions and A-type magmatism in the Tianshan and Altay orogens, NW China: Implications for geodynamic evolution and potential for the discovery of new ore deposits: Journal of Asian Earth Sciences, v. 32, p. 165–183.

Qin, K.Z., Ding, K.S., Xu, Y.X., Sun, H., Xu, X.W., Tang, D.M., and Mao, Q., 2007, Ore potential of protoliths and modes

of Co-Ni occurrence in Tulargen and Baishiquan Cu-Ni-Co deposits, East Tianshan, Xinjiang: Mineral Deposits, v. 26, p. 1–14 (in Chinese with English abstract).

Qin, K.Z., Fang, T.H., and Wang, S.L., 2002, Plate tectonics division, evolution and metallogenic settings in eastern Tianshan mountains, NW China: Xinjiang Geology, v. 20, p. 302–308 (in Chinese with English abstract).

Qin, K.Z., Zhang, L.C., Xiao, W.J., Xu, X.W., Yan, Z., and Mao, J.W., 2003, Overview of major Au, Cu, Ni and Fe deposits and metallogenic evolution of the eastern Tianshan Mountains, Northwestern China, in Mao, J.W., Goldfarb, R.J., Seltmann, R., Wang, D.W., Xiao, W.J., and Hart, C., eds., Tectonic evolution and metallogeny of the Chinese Altay and Tianshan: London, Natural History Museum, p. 227–249.

Ripley, E.M., 2009, Magmatic sulfide mineralization in Alaskan-type complexes, in Li, C.S., and Ripley, E.M., eds., New developments in magmatic Ni-Cu and PGE Deposits: Beijing, Geological Publishing House, p. 219–228.

Rublee, V.J., 1994, Chemical petrology, mineralogy and structure of the Tulameen Complex, Princeton area, British Colombia [Unpublished M.Sc. thesis]: University of Ottawa, Canada, p. 179.

Saleeby, J.B., 1992, Age and tectonic setting of the Duke Island ultramafic intrusion, southeast Alaska: Canadian Journal of Earth Science, v. 29, p. 506–522.

Sengör, A.M.C., Natal'in, B.A., and Burtman, V.S., 1993, Evolution of the Altaid tectonic collage and Paleozoic crustal growth in Asia: Nature, v. 364, p. 299–307.

Sengör, A.M.C., Natal'in, B.A., and Burtman, V.S., 2004, Phanerozoic analogues of Archean oceanic basement fragments: Altaid ophiolites and ophirags, in Kusky, T.M., ed., Precambrian ophiolites and related rocks: Amsterdam, Elsevier, p. 675–726.

Sha, L.K., 1995, Genesis of zoned hydrous ultramafic-mafic silicic intrusive complexes: An MHFC hypothesis: Earth Science Review, v. 39, p. 59–90.

Snoke, A.W., Quick, J.E., and Bowman, H.R., 1981, Bear Mountain igneous complex, Klamath Mountains, California: An ultrabasic to silicic calc-alkaline suite: Journal of Petrology, v. 22, p. 501–552.

Su, B.X., Qin, K.Z., Sakyi P.A., Li, X.H., Yang, Y.H., Sun H., Tang, D.M., Liu, P.P., Xiao, Q.H., and Malaviarachchi, S.P.K., 2010a, U-Pb ages and Hf-O isotopes of zircons from Late Paleozoic mafic-ultramafic units in southern Central Asian Orogenic Belt: Tectonic implications for an Early-Permian mantle plume: Gondwana Research, doi: 10.1016/j.gr.2010.11.015.

Su, B.X., Qin, K.Z., Sun, H., and Wang, H., 2010b, Geochronological, petrological, mineralogical and geochemical studies of the Xuanwoling mafic-ultramafic intrusion in the Beishan area, Xinjiang: Acta Petrologica Sinica, v. 26 , p. 3283–3294 in Chinese with English abstract).

Su, B.X., Qin, K.Z., Sun, H., Tang, D.M., Xiao, Q.H., and Cao, M.J., 2009, Petrological and mineralogical characteristics of Hongshishan mafic-ultramafic complex in Beishan area, Xinjiang: Implications for assimilation and fractional crystallization: Acta Petrologica Sinica, v. 25, p. 873–887 (in Chinese with English abstract).

Su, B.X., Zhang, H.F., Tang, Y.J., Chisonga, B., Qin, K.Z., Ying, J.F., and Sayki P.A., 2010c, Geochemical syntheses among the cratonic, off-cratonic and orogenic garnet peridotites and their tectonic implications: International Journal of Earth Sciences, doi: 10.1007/s00531-010-0527-0.

Sun, H., 2009, Ore-forming mechanism in conduit system and ore-bearing property evaluation for mafic-ultramafic complex in Eastern Tianshan, Xinjiang [Ph.D thesis]: Institute of Geology and Geophysics, Chinese Academy of Sciences (in Chinese with English abstract).

Sun, H., Qin, K.Z., Li, J.X., Xu, X.W., San, J.Z., Ding, K.S., Hui, W.D., and Xu, Y.X., 2006, Petrographic and geochemical characteristics of the Tulargen Cu-Ni-Co sulfide deposits, East Tianshan, Xinjiang, and its tectonic setting: Geology in China, v. 33, p. 606–617 (in Chinese with English abstract).

Sun, H., Qin, K.Z., Xu, X.W., Li, J.X., Ding, K.S., Xu, Y.X., and San, J.Z., 2007, Petrological characteristics and copper-nickel ore-forming processes of early Permian mafic-ultramafic intrusion belts in east Tianshan: Mineral Deposits, v. 26, p. 98–108 (in Chinese with English abstract).

Sun, M., Yuan, C., Xiao, W.J., Long, X.P., Xia, X.P., Zhao, G.C., Lin, S.F., Wu, F.Y., and Kröner, A., 2008, Zircon U-Pb and Hf isotopic study of gneissic rocks from the Chinese Altai: Progressive accretionary history in the early to middle Palaeozoic: Chemical Geology, v. 247, p. 352–383.

Tang, D.M., Qin, K.Z., Sun, H., Su, B.X., Xiao, Q.H., Cheng, S.L., and Li, J., 2009, Zircon U-Pb age and geochemical characteristics of Tianyu intrusion, East Tianshan: Constraints on source and genesis of mafic-ultramafic intrusions in East Xinjiang: Acta Petrologica Sinica, v. 25, p. 817–831 (in Chinese with English abstract).

Taylor, H.P., 1967, The zoned ultramafic complexes of southeastern Alaska, in Wyllie, P.J., ed., Ultramafic and related rocks: New York, Wiley, p. 97–121.

Thakurta, J., Ripley, E.M., and Li, C.S., 2008, Geochemical constraints on the origin of sulfide mineralization in the Duke Island Complex, southeastern Alaska: Geochemistry Geophysics Geosystems, v. 9, p. Q07003, doi: 10.1029/2008GC001982.

Valli, F., Guillot, S., and Hattori, K.H., 2004, Source and tectonometamorphic evolution of mafic and pelitic metasedimentary rocks from the central Quetico metasedimentary belt, Archean Superior Province of Canada: Precambrian Research, v. 132, p. 155–177.

Wang, J.B., Wang, Y.W., and He, Z.J., 2006, Ore deposits as a guide to the tectonic evolution in the East Tianshan Mountains, NW China: Geology in China, v. 33, p. 461–469 (in Chinese with abstract).

Wang, Y.W., Wang, J.B., Wang, L.J., and Long, L.L., 2009, Characteristics of two mafic-ultramafic rock series in the Xiangshan Cu-Ni-(V) Ti-Fe ore district, Xinjiang: Acta Petrologica Sinica, v. 25, p. 888–900 (in Chinese with English abstract).

Williams, H.R., 1991, Quetico subprovince: Geology of Ontario, v. 4, p. 383–403.

Windley, B.F., Alexeiev, D., Xiao, W., Kroner, A., and Badarch, G., 2007, Tectonic models for accretion of the Central Asian Orogenic Belt: Journal of Geological Society London, v. 164, p. 31–47.

Wu, S.M., Ma, R.S., Lu, H.F., Jia, D., and Cai, D.S., 1996, The Paleozoic tectonic evolution of the Western Tianshan, Xinjiang: Journal of Guilin Institute of Technology, v. 16, p. 95–101 (in Chinese with English abstract).

Xia, L.Q., Xu, X.Y., Xia, Z.C., Li, X.M., Ma, Z.P., and Wang, L.S., 2004, Petrogenesis of Carboniferous rift-related volcanic rocks in the Tianshan, northwestern China: Geological Society of America, v. 116, p. 419–433.

Xiao, Q.H., Qin, K.Z., Tang, D.M., Su, B.X., Sun, H., San J.Z., Cao, M.J., and Hui, W.D., 2010, Xiangshan composite

Cu-Ni-Ti-Fe and Ni-Cu deposit belongs to comagmatic evolution product: Evidence from ore microscopy, zircon U-Pb chronology and petrological geochemistry, Hami, Xinjiang, NW China: Acta Petrologica Sinica, v. 26, p. 503–522 (in Chinese with English abstract).

Xiao, W.J., Windley, B.F., Yuan, C., Sun, M., Han, C.M., Lin, S.F., Chen, H.L., Yan, Q.R., Liu, D.Y., Qin, K.Z., Li, J.L., and Sun, S., 2009, Paleozoic multiple subduction-accretion processes of the southern Altaids: American Journal of Sciences, v. 309, p. 221–270.

Xiao, W.J., Zhang, L.C., Qin, K.Z., Sun, S., and Li, J.L., 2004, Paleozoic accretionary and collisional tectonics of the eastern Tianshan (China): Implications for the continental growth of Central Asia: American Journal of Sciences, v. 304, p. 370–395.

Xiao, X.C., Tang, Y., Feng, Y., Zhu, B., Li, J., and Zhao, M., 1992, Tectonic evolution of Northern Xinjiang and its adjacent regions: Beijing, Geological Publishing House, p. 169 (in Chinese with English abstract).

Xu, X.Y., He, S.P., Wang, H.L., and Chen, J.L., 2009, Geological Background Map of Mineralization in Eastern Tianshan-Beishan Area (in Chinese).

Zhang, L.C., Qin, K.Z., and Xiao, W.J., 2008, Multiple mineralization events in the eastern Tianshan district, NW China: Isotopic geochronology and geological significance: Journal of Asian Earth Sciences, v. 32, p. 236–246.

Zhang, L.C., Qin, K.Z., Ying, J.F., Xia, B., and Shu, J.S., 2004, The relationship between ore-forming processes and adakitic rock in Tuwu-Yandong porphyry copper metallogenic belt, Eastern Tianshan mountains: Acta Petrologica Sinica, v. 20, p. 259–268 (in Chinese with English abstract).

Zhou, M.F., Lesher, C.M., Yang, Z.X., Li, J.W., and Sun, M., 2004, Geochemistry and petrogenesis of 270 Ma Ni-Cu-(PGE) sulfide-bearing mafic intrusions in the Huangshan district, Eastern Xinjiang, Northwest China: Implications for the tectonic evolution of the Central Asian Orogenic Belt: Chemical Geology, v. 209, p. 233–257.